CFP migration; practical aspects

Jan Thorbecke [1]

13.1 Introduction

In the past year the Common Focus Point (CFP) technology has become an important paradigm in the DELPHI research program. The interpretation and understanding of the CFP gathers has lead to significantly new insights and new processing schemes. In this Chapter the CFP technology and its applications are summarized and illustrated with examples of numerical and real data. The CFP imaging package, which was introduced in the previous DELPHI volume, has been developed, refined and implemented. The first results of the CFP package are shown in this chapter.

In section (13.2) the construction of a CFP gather and the applications of the CFP technology are explained and illustrated with simple numerical examples. Section (13.3) and section (13.4) show the imaging (double focusing process) on synthetic and field data.

13.2 CFP; definition, construction and application

The Common Focus Point (CFP) gather is constructed from seismic data acquired within a prespecified source aperture; the detector aperture follows from the detector spread(s)/streamers(s). To construct the CFP-gather from the data an initial synthesis operator is needed. This initial synthesis operator can be based on stacking velocities or an initial macro model. An initial synthesis operator is calculated by positioning a point source at the focus point followed by a forward modeling algorithm to calculate the source response at the surface. Measuring its response at the detector positions defines an operator for focusing in detection and measuring its response at the source positions defines an operator for focusing in emission. The synthesis op-

[1] E-mail: J.W.Thorbecke@CTG.TUDelft.NL

erator at the detector positions convolved in time with a shot record followed by a summation along all traces in the record defines one trace out of the CFP gather for focussing in detection. After the construction of the complete CFP gather the operator can be compared with the CFP gather and if necessary the model and/or the operator can be updated. In the comparison the operator must be coincident in time with the corresponding event in the CFP gather (principle of equal traveltime).

In the construction of a vertical time image there are two focusing steps involved; the first focusing step defines a focusing in detection and the second focusing step defines a focusing in emission. The second focusing step is a weighted stack of the CFP gather with its synthesis operator. In figure (13.1) this double focusing procedure is explained in a pictorial way. Note that the lateral position of the constructed single vertical time image is determined by the lateral position of the focus point. An alternative procedure can be obtained by placing the focusing result not at single vertical time but at double vertical time. This alternative procedure is shown in figure (13.2). In this chapter it will be shown that the double focusing concept is a very effective and efficient way of applying prestack migration.

13.2.1 CFP and $\mathbf{WRW}$

The focusing process can be expressed in the $\mathbf{WRW}$ matrix formulation of one-way wave propagation. The well known DELPHI model of seismic reflection data is given, for one reflector at z_m, by

$$\mathbf{P}^-(z_r) = \mathbf{D}^-(z_r)\mathbf{W}^-(z_r, z_m)\mathbf{R}^+(z_m)\mathbf{W}^+(z_m, z_s)\mathbf{S}^+(z_s) \tag{13.1}$$

where z_r are the receiver positions, z_m the position of the reflector and z_s represents the source position. Note that z_r, z_s and z_m are in general a function of x. Focusing is defined by a weighted (in phase and amplitude) summation along the source or receiver arrays in such a way that the constructed wave front has a focus point in the subsurface. The weighting operator is also called the synthesis operator. The principle of combining shot gathers at the surface, also called areal shot record technology, was already introduced by Berkhout (1992) for controlled illumination in prestack depth migration. Rietveld (1995) has shown many examples for the planar areal sources.

The focusing operator for the receiver arrays, applied to the left side of the right-hand side of equation (13.1), is defined as

$$\vec{\Gamma}_i^-(z_r)\mathbf{D}^-(z_r)\mathbf{W}^-(z_r, z_m) = \vec{I}_i^-(z_m) \tag{13.2}$$

$$\vec{\Gamma}_i^-(z_r) \approx \vec{I}_i^-(z_m)\left[\mathbf{W}^+(z_m, z_r)\right]^*\left[\mathbf{D}^-(z_r)\right]^{-1} \tag{13.3}$$

with $\vec{I}_i^-(z_m)$ a unit vector with a 1 at the i^{th} position at depth z_m and $\Gamma_i^-(z_r)$ the focusing operator at the receiver positions at the surface (see figure (13.3)). Note that the approximation sign in equation (13.2) refers to the approximation of the inverse of the propagation operator $\mathbf{W}^-(z_r, z_m)$ with its matched filter $\left[\mathbf{W}^-(z_r, z_m)\right]^{-1} \approx \left[\mathbf{W}^+(z_m, z_r)\right]^*$.

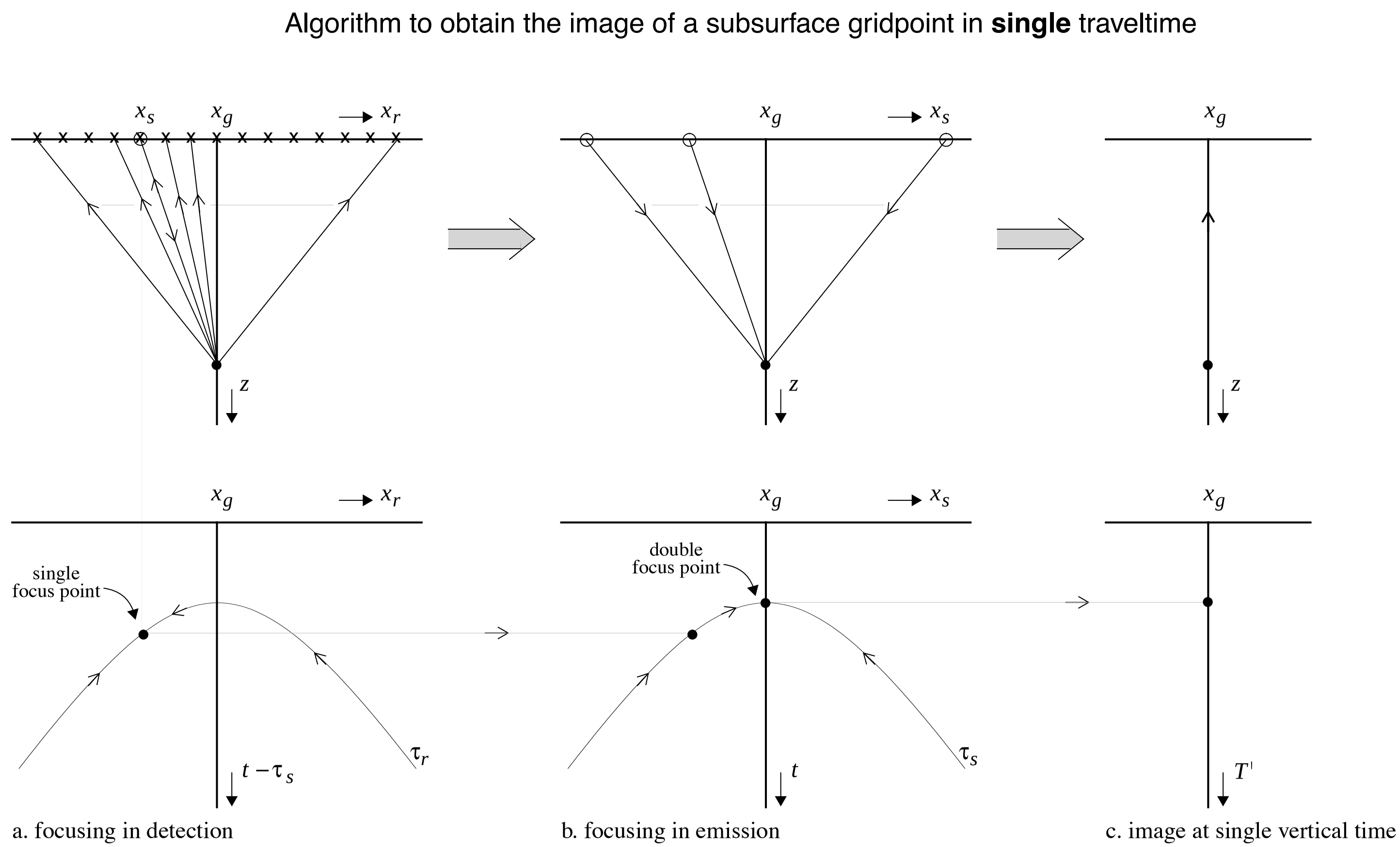

Fig. 13.1 *Focusing of the gridpoint-related backscattered energy in each shot record (focusing in detection) involves integration along the delayed focusing operator, the delay being given by the source-gridpoint traveltime; the focusing result is positioned below the* **source** *location and located at the source-gridpoint single traveltime. Using all shot records within a given aperture, the output of focusing in detection represents the gridpoint-related focus point response in single traveltime. Subsequent focusing of the gridpoint-related illumination energy involves integration along the focus point response (focusing in emission); the double focusing result is positioned below the* **gridpoint** *location at the single vertical time (T').*

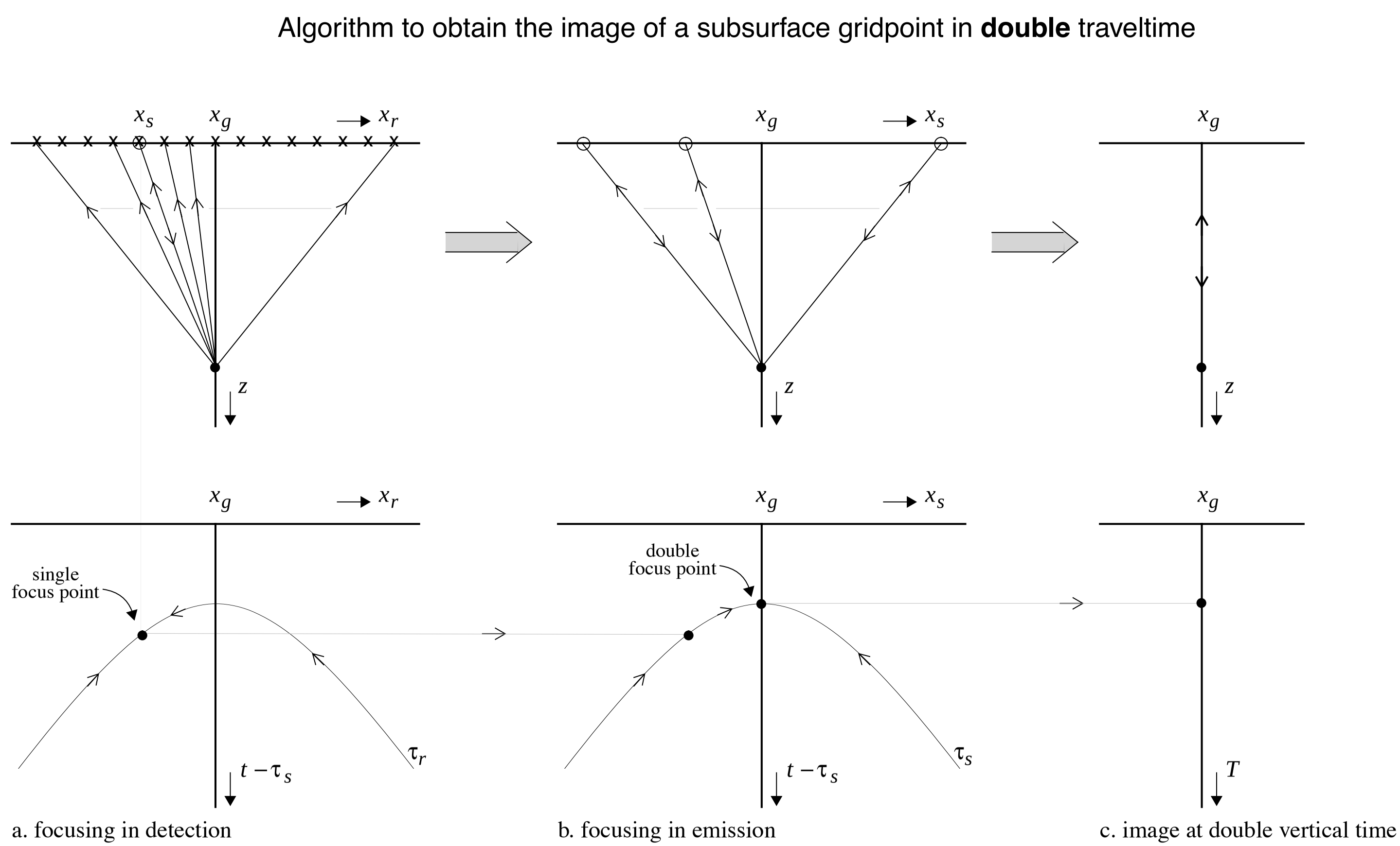

Fig. 13.2 *Focusing of the gridpoint-related backscattered energy in each shot record (focusing in detection) involves integration along the delayed focusing operator, the delay being given by the source-gridpoint traveltime; the focusing result is positioned below the* **source** *location at the source-gridpoint double traveltime. Using all shot records within a given aperture, the output of focusing in detection represents the gridpoint-related focus point response in double traveltime. Subsequent focusing of the gridpoint-related illumination energy involves integration along the double traveltime focus point response (focusing in emission); the double focusing result is positioned below the* **gridpoint** *location at the double vertical time (T).*

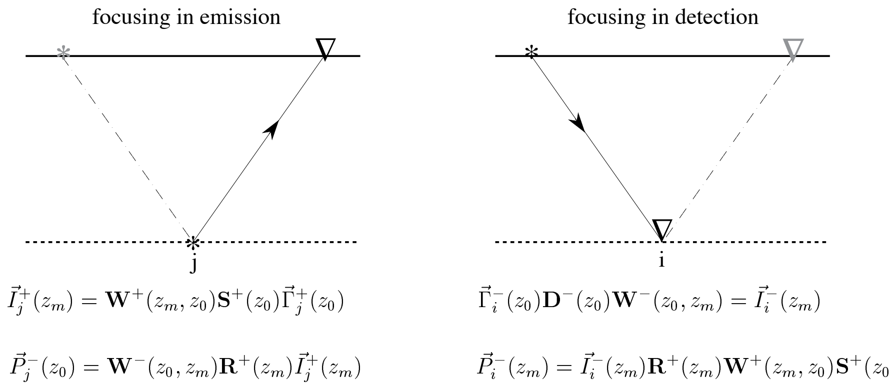

Fig. 13.3 *Focusing in detection places a notional areal receiver on a reflecting boundary and focusing in emission places a notional areal source on a reflecting boundary.*

The focusing operator for the source arrays, applied to the right side of the right-hand side of equation (13.1), is defined as

$$\vec{I}_j^+(z_m) = \mathbf{W}^+(z_m, z_s)\mathbf{S}^+(z_s)\vec{\Gamma}_j^+(z_s) \tag{13.4}$$

$$\left[\mathbf{S}^+(z_s)\right]^{-1}\left[\mathbf{W}^-(z_s, z_m)\right]^* \vec{I}_j^+(z_m) \approx \vec{\Gamma}_j^+(z_s) \tag{13.5}$$

with $\vec{I}_j^+(z_m)$ a unit vector with a 1 at the j^{th} position at depth z_m and $\vec{\Gamma}_j^+(z_s)$ the focusing operator at the source positions (see figure (13.3)). The focusing operators $\Gamma^{\pm}$ perform a summation along the receiver positions ($\vec{\Gamma}^-$) in a common shot gather or a summation along the source positions ($\vec{\Gamma}^+$) in a common receiver gather. This summation (or synthesis) is carried out for all source and receiver positions available.

Substituting equation (13.2) into equation (13.1) gives an expression of the data after focusing of the detector array

$$\vec{\Gamma}_i^-(z_r)\mathbf{P}^-(z_r) = \vec{P}_i^-(z_r) = \vec{I}_i^-(z_m)\mathbf{R}^+(z_m)\mathbf{W}^+(z_m, z_s)\mathbf{S}^+(z_s) \tag{13.6}$$

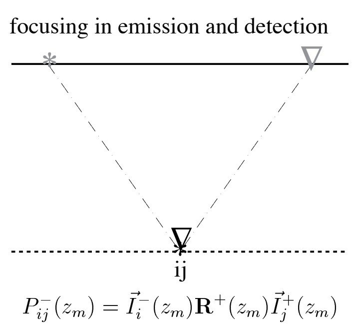

Fig. 13.4 *Focusing in detection and emission places a notional areal source and a notional areal receiver on a reflecting boundary.*

where equation (13.6) is an expression for the Common Focus Point (CFP) gather for detection. Substituting equation (13.4) into equation (13.1) gives an expression for the focusing of the source array

$$\mathbf{P}^-(z_r)\vec{\Gamma}_j^+(z_s) = \vec{P}_j^-(z_r) = \mathbf{D}^-(z_r)\mathbf{W}^-(z_r, z_m)\mathbf{R}^+(z_m)\vec{I}_j^+(z_m) \tag{13.7}$$

where equation (13.7) is an expression for the Common Focus Point (CFP) gather for emission.

Focusing of both the detector and the source array by combining equation (13.2) and equation (13.4) into equation (13.1) gives

$$P_{ij}^-(z_r) = \vec{\Gamma}_i^-(z_r)\mathbf{P}^-(z_r)\vec{\Gamma}_j^+(z_s) = \vec{I}_i^-(z_m)\mathbf{R}^+(z_m)\vec{I}_j^+(z_m) = R_{ij}^+(z_m) \tag{13.8}$$

which is the double focus result shown in figure (13.4).

13.2.2 Construction of CFP's

The construction of a CFP gather is explained by following the steps explained in the previous section. For this purpose numerical data, based on the model shown in figure (13.5)a, is used. The numerical data is modeled with a fixed acquisition spread where the source positions are defined at every receiver position (201 shot positions with $\Delta x = 15m$). The source has a dipole character and its signature is given by a Ricker wavelet with a frequency peak at 26.4 Hz. For the modeling an acoustic finite difference algorithm is used. The subsurface model includes a diffraction point at $z = 1000$, $x = -750$ m and a negative reflection coefficient for the wedge in the right corner of the model. Explaining the CFP processing techniques in the next sections is done with the use of this syncline model. The synthesis process for a focusing receiver with a focus point defined at the synclinal interface at $x = 0$ and $z = 950m$ (the focus point is indicated with a black bullet in figure (13.5a)) is shown in detail in figure (13.5).

The time reversed focusing operator $\vec{\Gamma}_i^-(z_r)$ for the defined focus point is shown in figure (13.5b). This operator is applied to all common shot gathers available. Three different common shot gathers with source positions at $x = -495, z = 0$ and $x = 495$ are shown in figure (13.5) c, d and e respectively. Convolution along the time axis of the traces in the shot gathers with the traces in the synthesis operator gives the intermediate synthesis results shown in figure (13.5) f, g and h. Note that in these intermediate synthesis results the bow-tie of the syncline structure is still present. Summation over all the traces in the intermediate synthesis result gives one trace of the CFP gather. The most important contribution in the summation result is determined by the Fresnel zone. The lateral position of the centre of the Fresnel zone is determined by following the ray-path from the source, via the focus point position, to the receiver position. Thus for a 1-Dimensional medium the Fresnel zone is given by the source position mirrored in the focus point position. The time position of the Fresnel zone contribution of the event of interest is indicated by the time of the synthesis operator at the source position. If the focusing operator is correct then the time given by the operator is identical with the time in the CFP gather (for a detailed discussion see DELPHI volume VI Chapter 10). The summed

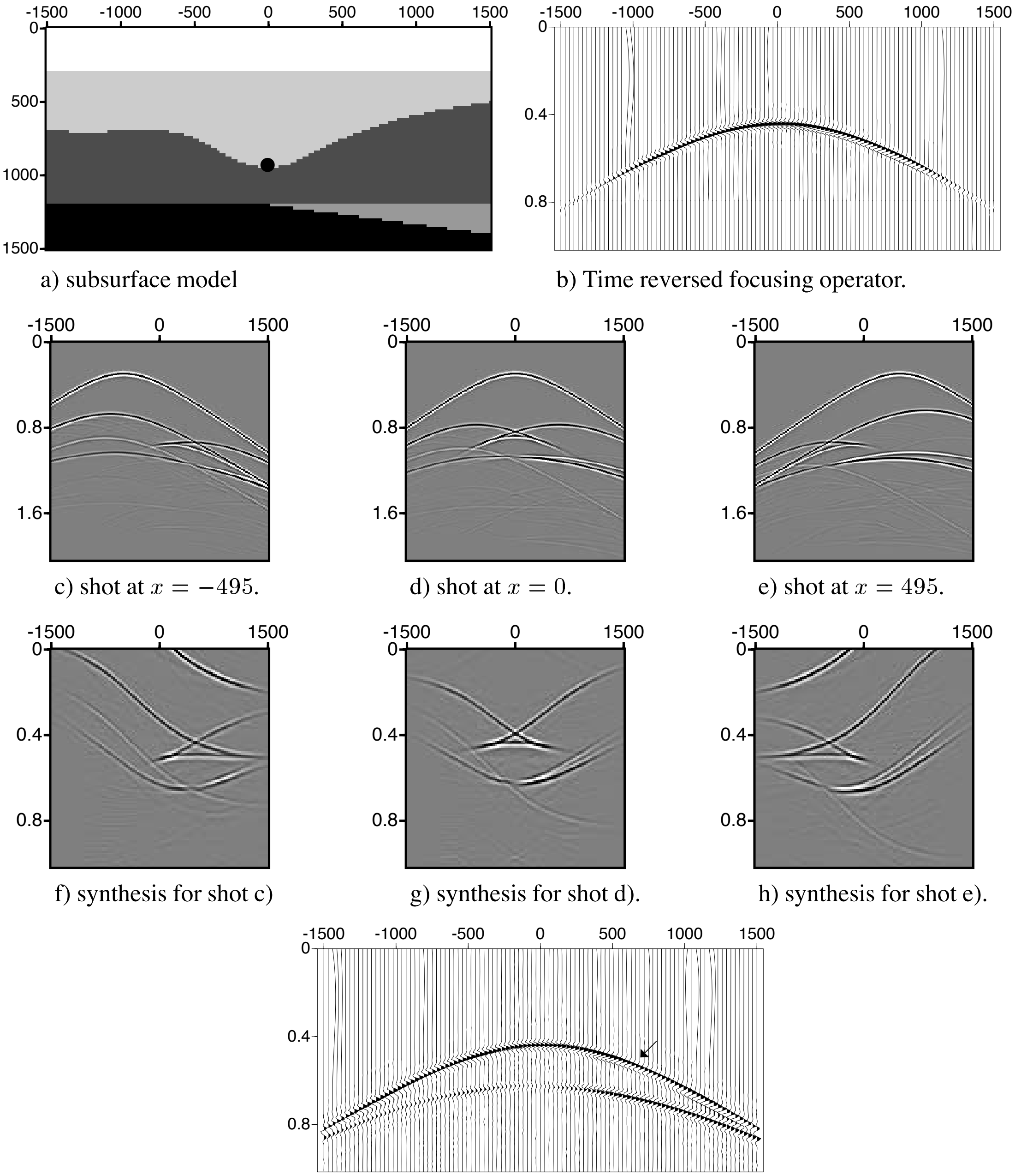

a) subsurface model

b) Time reversed focusing operator.

c) shot at $x = -495$.

d) shot at $x = 0$.

e) shot at $x = 495$.

f) synthesis for shot c)

g) synthesis for shot d).

h) synthesis for shot e).

i) CFP gather.

Fig. 13.5 *Construction of a CFP gather for focusing in detection. Every common shot gather contributes to one trace, positioned at the source position, in the CFP gather. Note the contribution of the Fresnel zones in figure (13.5)f,g and h to figure (13.5)i. The focus point response has been indicated with an arrow. Note the relative simplicity of the CFP gather.*

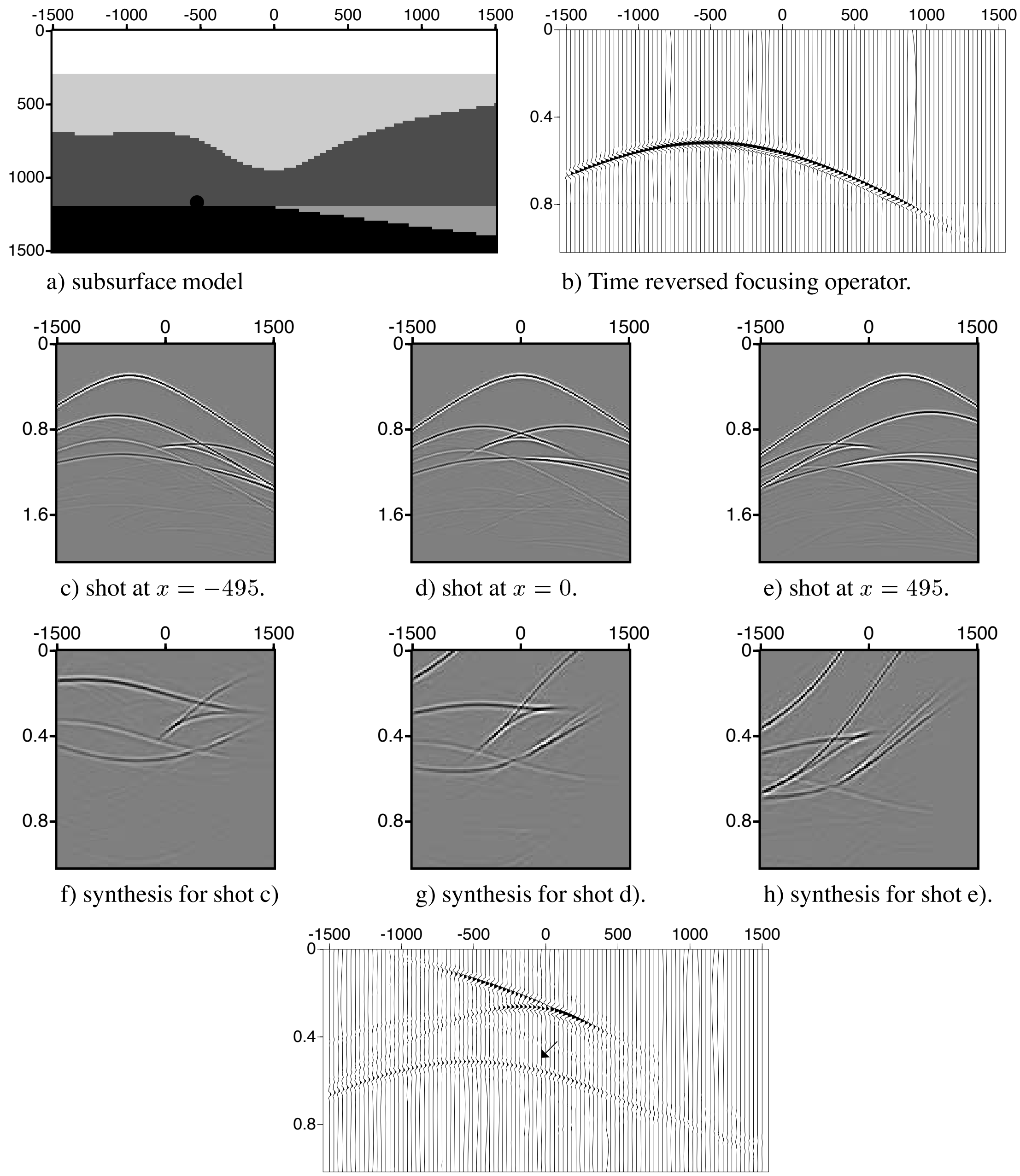

a) subsurface model

b) Time reversed focusing operator.

c) shot at $x = -495$.

d) shot at $x = 0$.

e) shot at $x = 495$.

f) synthesis for shot c)

g) synthesis for shot d).

h) synthesis for shot e).

i) CFP gather.

Fig. 13.6 *Construction of a CFP gather for focusing in detection. Every common shot gather contributes to one trace, positioned at the source position, in the CFP gather. Note the contribution of the Fresnel zones in figure (13.6)f,g and h to figure (13.6)i. The focus point response has been indicated with an arrow. Note the relative simplicity of the CFP gather.*

trace is placed in the CFP gather at the position of the source. By carrying out the convolution and integration along the traces in the gather for all shot gathers the CFP gather for a focusing detector is constructed.

The events which are present in the shot record are also present in the intermediate synthesis result in figure (13.5)f, g and h. In figure (13.5)f four events are observed, the top event originates from the first reflector and can be regarded as a non-causal event because we have placed the source below the first reflector. The event with the triplication in it originates from the syncline boundary, the weak S-shaped event originates from the diffraction point and the last event originates from the deepest boundary. In the CFP gather shown in figure (13.5)i the reflection from the syncline and the deeper boundary are clearly visible. The response of the first reflector is moved outside the time window. Note that the bow-tie event in the two-way time shot gather (figure (13.5d)) is focused in the CFP gather (figure (13.5i)) and is therefore much simpler to interpret. In the construction of a CFP gather the shot records are transformed to an another shot record which is less complicated.

Figure (13.6) shows the construction of a CFP gather for a focus point at the deep boundary at $x = -500$. In the CFP in (13.6)i a strong non-causal event is present which originates from the syncline interface. It is possible to remove this non-causal event from the CFP gather by zeroing the samples above the operator times. In standard use of the CFP gather the 'non-causal' events are muted out the CFP gather.

The event in the CFP gather of figure (13.5i) corresponding to the synthesis operator is exactly equal in traveltime with the synthesis operator, which means that the constructed synthesis operator contains no errors. If the source and receivers are defined at the same positions in space the same synthesis operator can be used for the second focusing step, focusing in emission, operating on the CFP gather. In subsection 13.2.7 this second focusing step is discussed in more detail. If the synthesis operator is not equal in traveltime with the event of interest in the CFP gather the synthesis operator needs to be updated (chapter 9). Note that by updating synthesis operators (and not the initial macro model) a correct vertical time image of the subsurface can be obtained without using a macro model. To convert this vertical time image to a structural

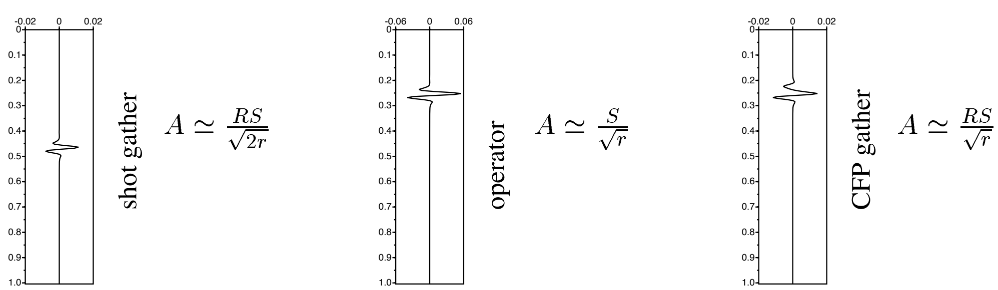

Fig. 13.7 *Amplitudes of a trace from a shot gather, synthesis operator and CFP gather, where S represents the amplitude of the wavelet, R the reflection coefficient at 45^o and r the distance between the focus point and the receiver at the surface.*

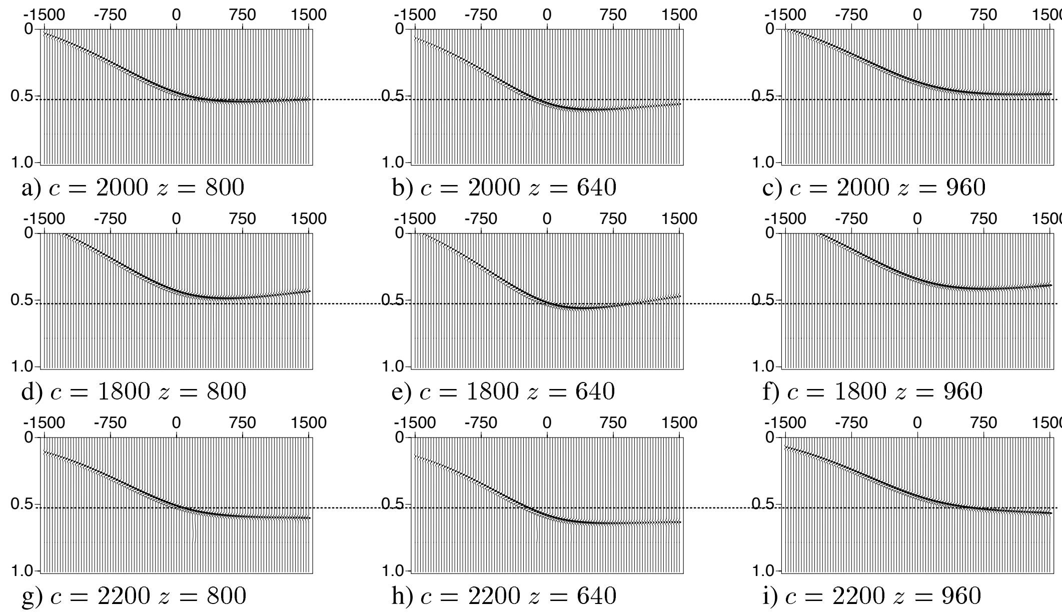

Fig. 13.8 *Construction of a trace in the CFP gather for a flat reflector with different erroneous operators. The shot record used is the 75^{th} shot ($x = -750$) in a fixed acquisition geometry.*

model (a depth image) a macro model is needed. This macro model can be estimated by using the collection of synthesis operators and the obtained vertical time image. The conversion from vertical time to depth involves time shifts along the time axis only.

The amplitudes present in the CFP gather can be interpreted by looking at the construction of the CFP gather for the top flat layer in figure (13.5a). The synthesis operator is defined for a focus point at the reflector at $x = 0$ and $z = 300$ m. The stationary phase contribution in the CFP gather of the shot record with a source position at $x = -300$ is given by the trace at $x = 300$ (mirrored around $x = 0$). This stationary phase trace is shown at the left side of figure (13.7). The amplitude in this trace consists of $\frac{RS}{\sqrt{2r}}$, where S represents the amplitude of the wavelet, R the reflection coefficient at 45^o and r the distance between the focus point and the receiver at the surface (in the given example $r = \sqrt{2 * 300^2}$). The operator trace at $x = 300$, the middle trace in figure (13.7), has an amplitude proportional to $\frac{S}{\sqrt{r}}$. The right trace in figure (13.7) represents the contribution of the shot gather in the CFP gather. The amplitude in the CFP gather is proportional to $\frac{RS}{\sqrt{r}}$. Dividing (in a least squares sense) the CFP gather by its synthesis operator gives the reflection coefficient for an angle of incidence of 45^o. This relation ship between the CFP gather and the synthesis operator can be used to determine the AVO behavior at the focus point (see chapter 9 of this volume).

Using an erroneous operator will give a different construction of the CFP gather. This is shown in figure (13.8) for several errors in the synthesis operator for a shot record with a source position at $x = -750$ (the 75^{th} out of a range of 301 shot records) in a 1 dimensional medium with a fixed acquisition spread. The reflector in the 1 dimensional medium is positioned at 800 m

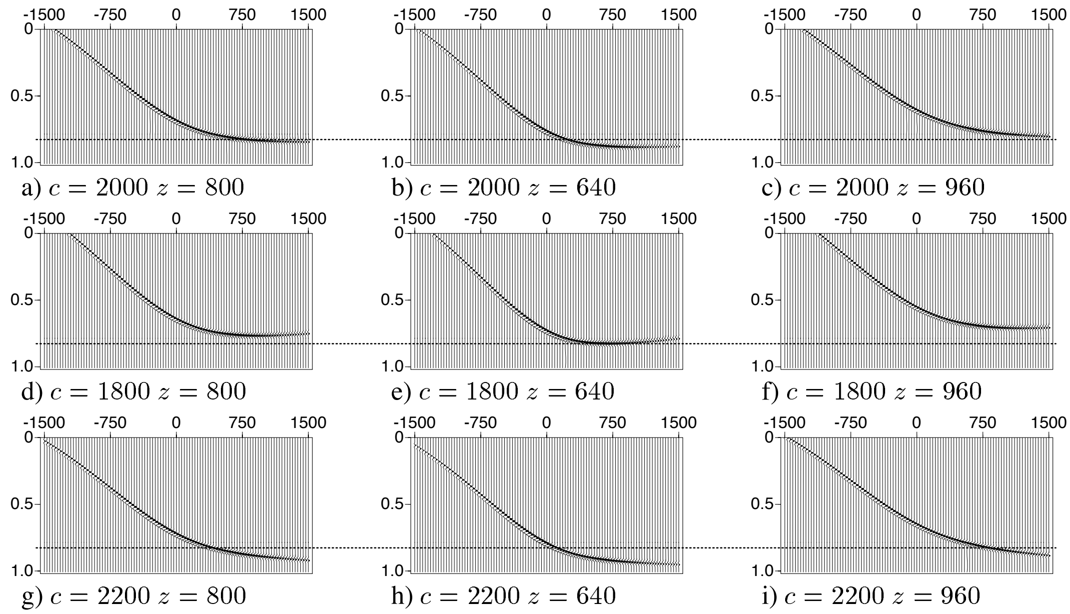

Fig. 13.9 *Construction of a trace in the CFP gather for a flat reflector with different erroneous operators. The shot record used is the first shot ($x = -1500$) in a fixed acquisition geometry.*

depth and the velocity of the first layer is $2000 m/s$. The CFP gathers constructed with the erroneous synthesis operators are shown in figure (13.10). Note that the 75^{th} trace (at $x = -750$) of the CFP gather in figure (13.10) is the summation along the traces of figure (13.8). The introduced errors in the synthesis operators give CFP gathers which are not coincident in traveltime with the operator. In figure (13.8), where the correct time is given by the dotted line, it is observed that the Fresnel zone is shifted due to the error in the operator. This shift in the Fresnel zone can disturb the final summation when the Fresnel zone is shifted out of the aperture range. In figure (13.9) the same erroneous operators are used but now for a shot with a source position at $x = -1500$, which gives the first trace at $x = -1500$ in the CFP gathers shown in figure (13.10).This shot record is positioned at the edge of the model and the Fresnel zone can be shifted out of the aperture range due to an erroneous operator.

If the Fresnel zone for an erroneous operator stays within the aperture range then the CFP gather can be corrected for the erroneous operator and the calculation of a new synthesis with an updated operator is not necessary. It is therefore advantageous to look at methods which keep the Fresnel zone within the aperture range. In figure (13.9)g, h and i we observe that the Fresnel zone is shifted outside the aperture range due to the error in the operator. The first synthesis process may be improved if not only one trace for the CFP gather is calculated and used but also neighboring traces of different CFP gathers, constructed with a lateral shifted operator, are used. In figure (13.11) the first shot record with a source at $x = -1500$, corrected with an erroneous synthesis operator also used in (13.9)i, is shown for different lateral shift in the synthesis operators. Now it is observed that the Fresnel zone which is shifted out of the aperture range due to an erroneous operator, can be included in the CFP gather by shifting the operator

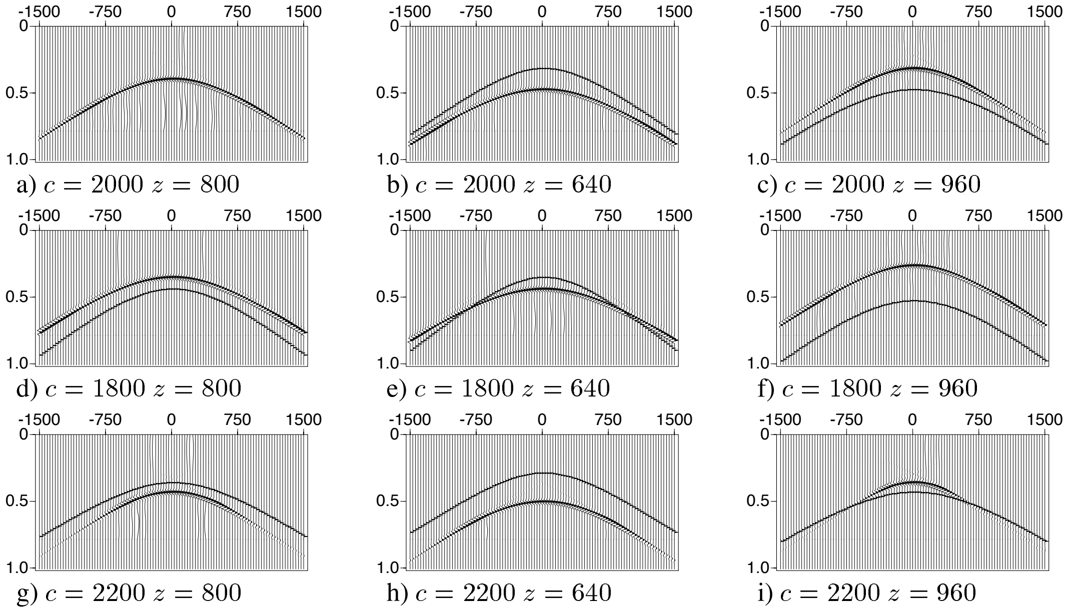

Fig. 13.10 *CFP gathers for a flat reflector with different erroneous operators. The shot records are simulated in a fixed acquisition geometry.*

laterally and using these results in the construction of the CFP gather. Note that the laterally shifted synthesis operators bring the Fresnel zone back in the aperture range at a different time and with a different amplitude after summation. Note also that in considering all possible laterally shifted operators within the aperture range means that a 2 dimensional cross-correlation is carried out between the data and the synthesis operator.

The 2-dimensional convolution between the CFP gather and its synthesis operator is shown in figure (13.12) for different erroneous synthesis operators. The time and offset of the convo-

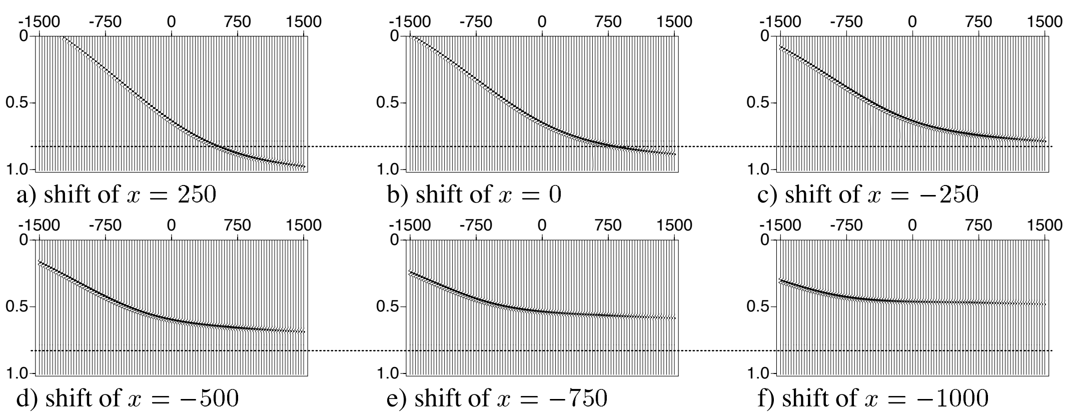

Fig. 13.11 *1 Dimensional cross-correlation between laterally shifted erroneous operators (*$c = 2200$ $z = 960$*) and one shot record at* $x = 0$.

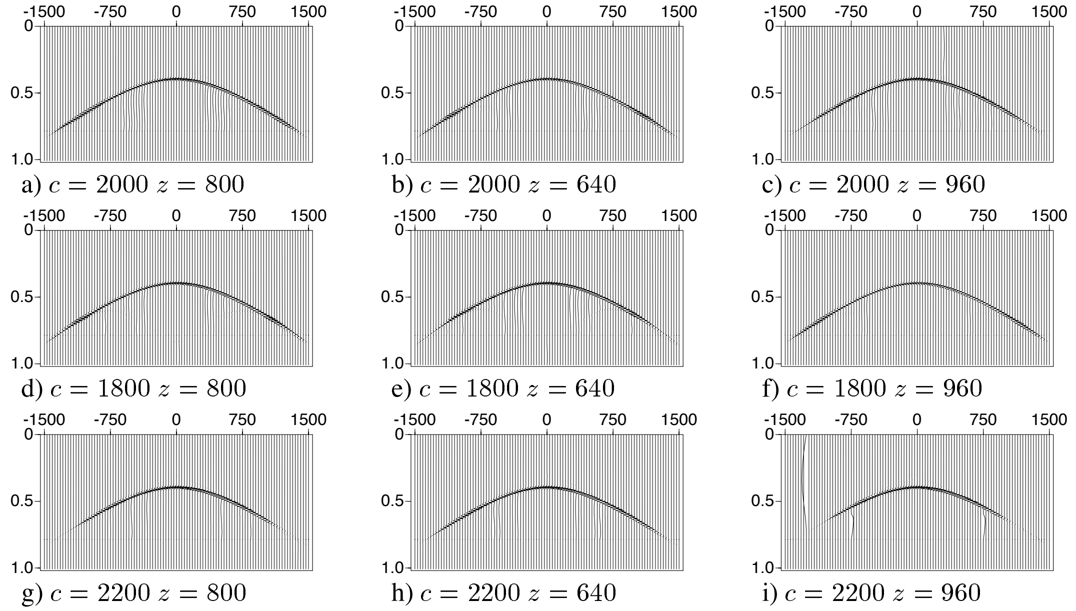

Fig. 13.12 *2-Dimensional convolution between the CFP gather and its operator for different erroneous operators. Note that all convolutions give the same result, meaning that erroneous CFP gathers can be automatically updated.*

lution results are displayed by halving the original spatial and time sampling rate. Note that all convolutions are identical in traveltime with the correct synthesis operator. The error introduced in the CFP gather due to an erroneous operator is compensated in the 2-dimensional convolution. Note also that the amplitude differences in the different convolution results is not significant. This means that the wavelet is not distorted by the use of an erroneous operator, in the first focusing process.

Adding noise to the data will distort the CFP but due to the summation of the events in the Fresnel zone the signal to noise ratio is improved compared with the shot records the CFP is build from. This is illustrated in figure (13.13) where noise is added to the shot records. Subtracting the noise free CFP from the noisy CFP shows only the finite aperture effects. This means that the Fresnel zone is not strongly disturbed by the noise in the data.

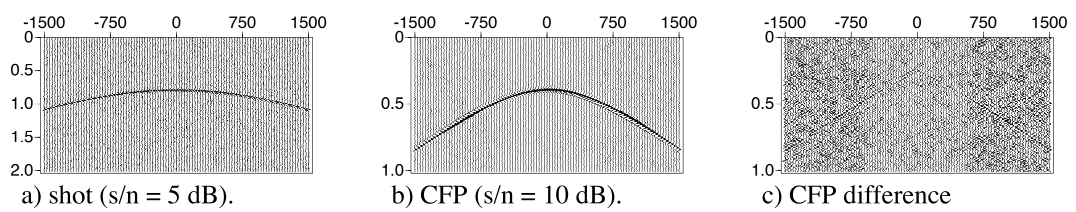

Fig. 13.13 *Signal enhancement due to the construction of the CFP gather. The scaling in figure a and b are the same.*

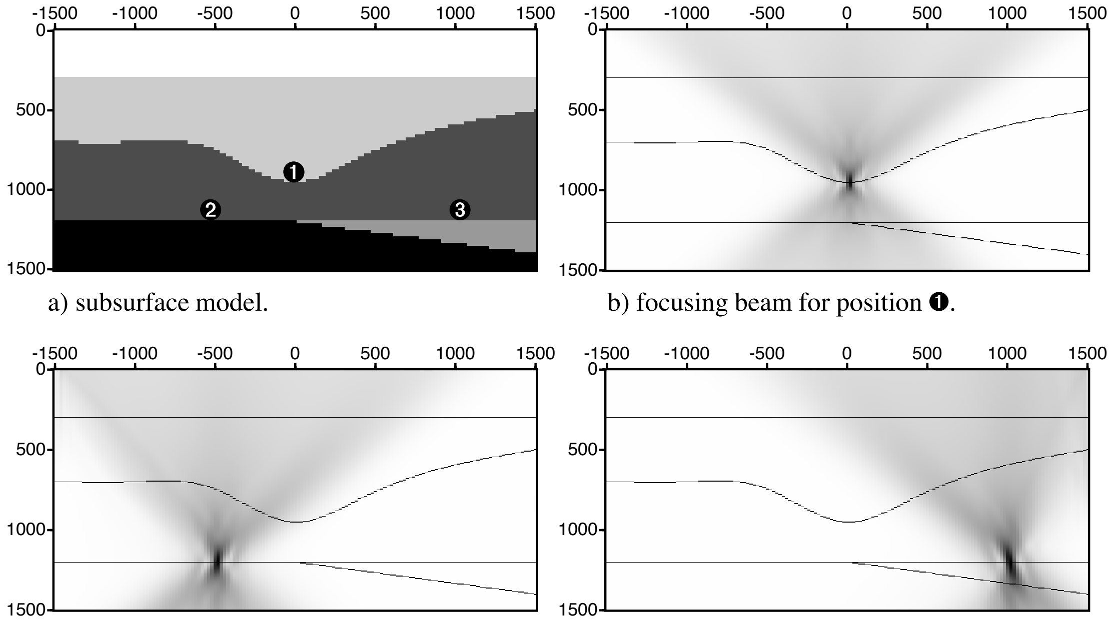

a) subsurface model.

b) focusing beam for position ❶.

c) focusing beam for position ❷.

d) focusing beam for position ❸.

Fig. 13.14 *Focusing beams through the subsurface model given in a). Note the tube like shape of the different focusing areas.*

13.2.3 Resolution analysis with focusing beams

Modeling the energy of the propagating waves of the synthesis operator through the subsurface model gives an indication how the areas in the subsurface are illuminated by this synthesis operator and which aperture at the surface is most important for the illumination. With these illumination areas the distribution of the focus points in the subsurface can be determined in order to obtain an efficient and optimum illumination of the subsurface. In figure (13.14) three focusing beams are shown for the syncline model introduced in the previous section. The beams are constructed by performing a recursive depth extrapolation of the focusing operators through the model and calculating at every depth step the energy of the wavefield as function of the lateral position. Note that for the construction of the beams only the synthesis operators and a macro model are needed.

From the focusing beams in figure (13.14) it can be seen that around the actual focus point most of the energy is focused in a tube like shaped area. In the beams shown in figure (13.14) the tube has a lateral extent which is smaller than the vertical extent. The extension of the focusing area is related to the resolution at the focusing point. The lateral and vertical resolution of a focus point is determined by the acquisition geometry and the subsurface model. By using the information of the focusing beams it is possible to define at which sampling density the focus points have to be chosen to illuminate the subsurface properly.

Zooming in at the focus point of figure (13.14c) in figure (13.15) shows that the focusing area is not limited to the defined focus point but has an extension in the horizontal and vertical direc-

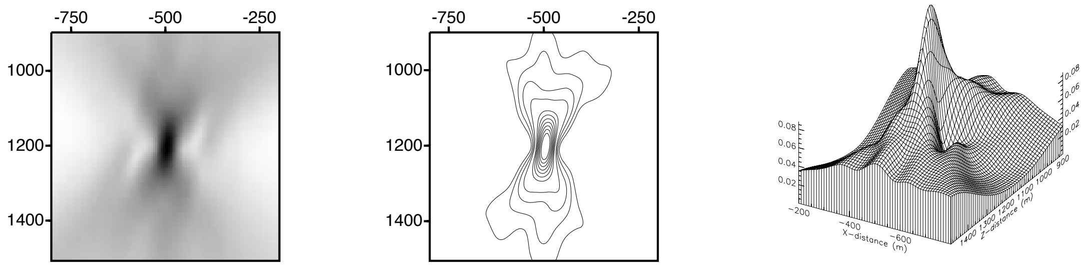

a) grayscale plot. b) contour plot. c) 3D plot.

Fig. 13.15 *Details for focusing position 2 of figure (13.14c). Note that the focusing area is not limited to the defined focus point at $x = -500$, $z = 1200$ m.*

tion. In the contour plot, plotted with equidistant contour values, it is observed that the inner contour lines are close together. In the 3D plot this is observed as a broad peak at the focus point position. With these observations the focus point distribution can be determined. For example a good illumination in the horizontal direction can be obtained by putting at every 50 m a focus point and a good illumination in the vertical direction can be obtained by putting a source at every 100 m.

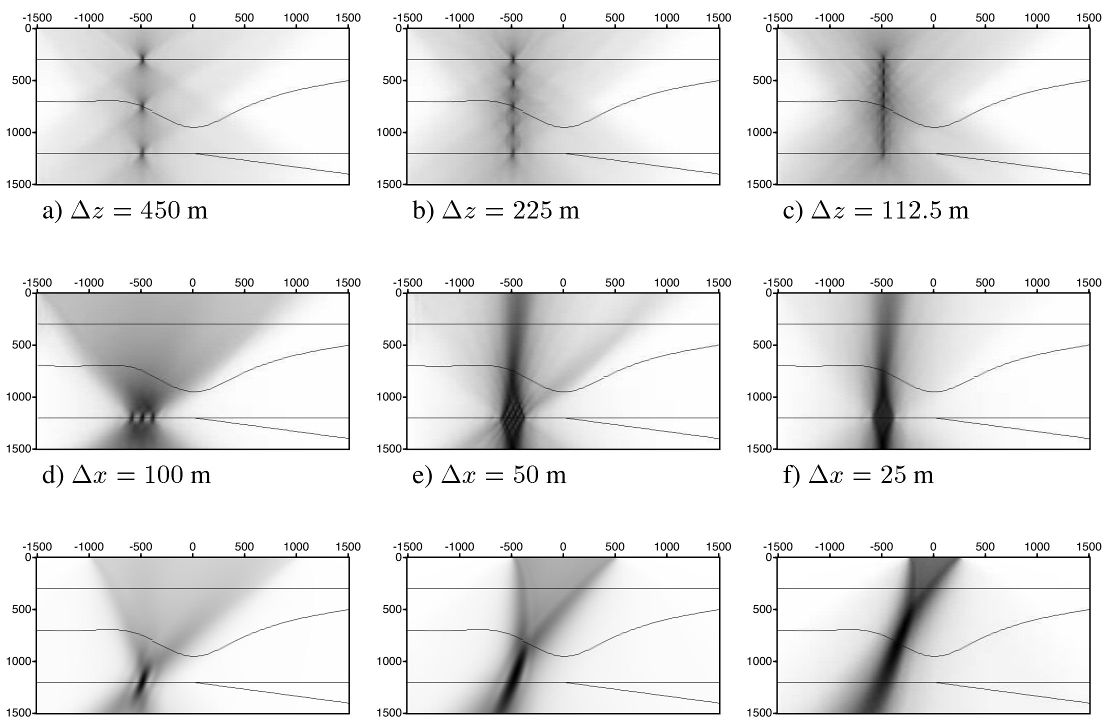

a) $\Delta z = 450$ m b) $\Delta z = 225$ m c) $\Delta z = 112.5$ m

d) $\Delta x = 100$ m e) $\Delta x = 50$ m f) $\Delta x = 25$ m

g) aperture $= 2000$ m h) aperture $= 1000$ m i) aperture $= 500$ m

Fig. 13.16 *Different focus point densities in lateral and vertical position. Note that for a complete illumination a sparse distribution of the focus points is sufficient.*

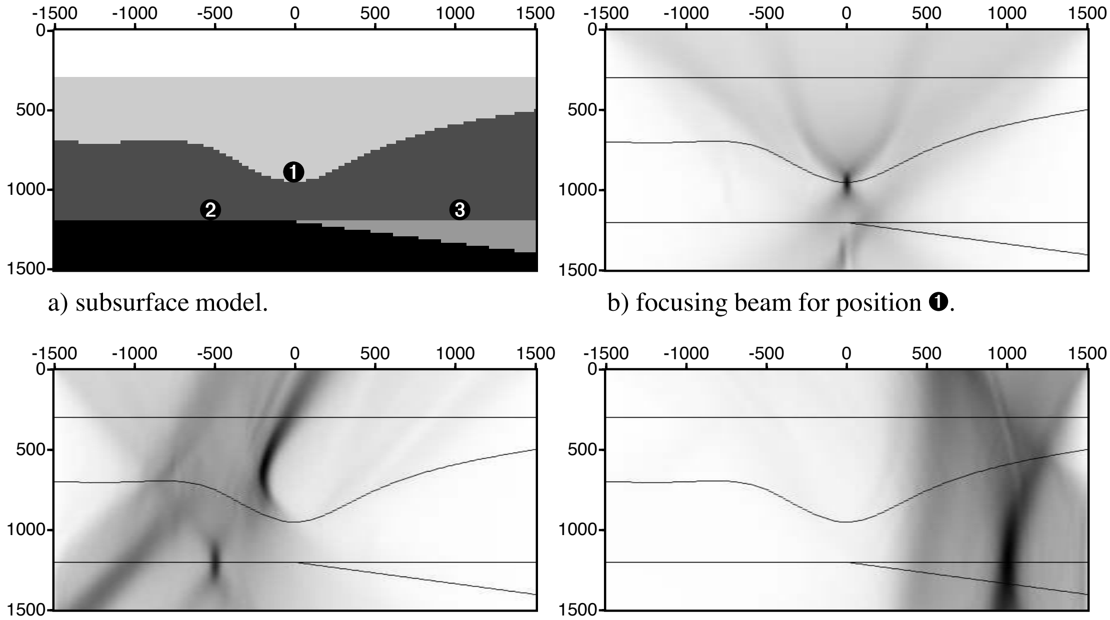

a) subsurface model.

b) focusing beam for position ❶.

c) focusing beam for position ❷.

d) focusing beam for position ❸.

Fig. 13.17 *Focusing beams of CFP gathers extrapolated through the subsurface model given in a). Note that there are more focusing areas than in figure (13.14).*

In figure (13.16) different combinations of focusing operators are used to illuminate the subsurface. Placing, at the same lateral position in the model, three focus point (one at every boundary) gives the illumination shown in figure (13.16a). This illumination is not sufficient to illuminate the events in-between the boundaries. Reducing the distance between the focus point gives the results shown in figure (13.16b) and (13.16c). From these experiments it can be concluded that in the first focusing process focus points distributed with a vertical distance of ± 100 m are sufficient to illuminate the events in-between the focus points correctly. This is of significant importance for efficiency, particularly in 3-D.

The horizontal distance between the focus points must be chosen smaller than the vertical distance to obtain a sufficient illumination. In figure (13.16d), (13.16e) and (13.16f) three different horizontal focus point distributions are shown. By limiting the operator aperture the focusing beams become lateral broader as shown in figure (13.16g), (13.16h) and (13.16i). So by limiting the operator aperture (which means reducing the maximum angle which can be focused) a broader focusing beam is obtained which gives a less accurate image, but it can be obtained by using less operators.

The introduced analysis with focusing beams are a helpful tool in determining the focus point distribution in the subsurface. The focusing beams give more information than ray-tracing, because the resolution of the focusing energy is shown as well. The same algorithm can also be used by monitoring the focusing of the events present in the constructed CFP gather. In figure (13.17) the focussing beams are shown for the CFP gathers constructed with the operators of figure (13.14). At the defined focus point the focusing is the same as the focusing of the operators. Note that due to the angle dependent reflection coefficient (which is present in the CFP gather) in figure (13.17b) the focusing of the CFP gives a slightly different focussing pattern as in figure (13.14b). Beside the defined focus point other focus point are also visible. Below the main focus point in figure (13.17b) there are two more focus point visible which originate from the deeper reflections. However these focus points are not positioned correctly. Figure (13.6)i shows the CFP gather used in the calculation of the beam in figure (13.17c). In figure (13.17c) a strong focusing area is present above the defined focussing position. The strong 'non-causal' event in the CFP gather above the traveltime of the operator gives rise to this strong focusing area. This area cannot be interpreted because it originates from a 'non-causal' event present in the CFP gather. It is included in this example to show that the non-causal events should be muted out if one wants to make beams out of CFP gathers. In figure (13.17d) the defined focusing area is extended to the deeper layer to to the presence of the deeper reflector.

13.2.4 Traveltime and Ray paths

In (Parkes and Hatton, 1987) the image ray is defined as "the ray associated with the minimum traveltime from a subsurface point to the surface. Time migration of data has the effect of moving points laterally to their minimum time positions, rather than their 'true' time positions. The normal ray is associated with the minimum traveltime from a coincident source/receiver pair to any particular interface. Depth migration of data has the effect of moving points along their image ray to their correct position. By definition the normal ray is perpendicular to the target interface and the image ray is perpendicular to the surface."

By the CFP technology a new ray is introduced: the, generally bended, vertical ray. The vertical ray is associated with the traveltime of a source in the subsurface to a receiver at the same lateral position at the surface. In figure (13.18) the vertical ray is displayed together with the image ray and the normal ray (in order to observe the difference between the different ray paths better the velocities of the syncline model are modified). Note that for a correct imaging of the normal and image rays a lateral shift of the data points is needed. In the CFP imaging procedure

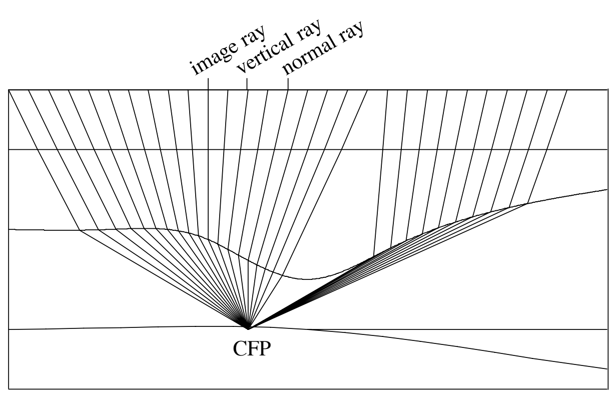

Fig. 13.18 *Vertical, normal and image ray for a focus point in the subsurface in the syncline model.*

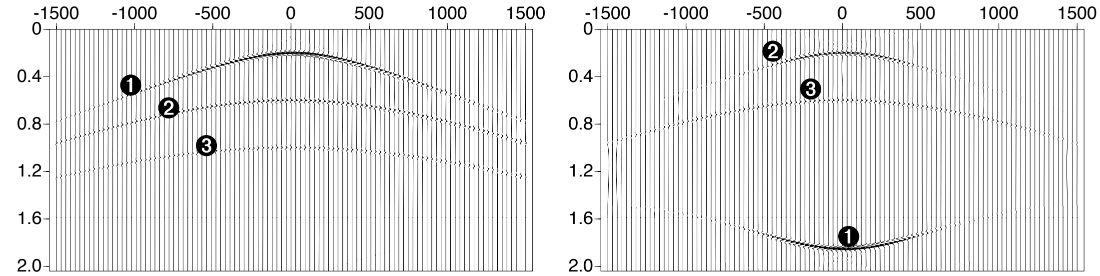

a) CFP gather for first reflector. b) CFP gather for third reflector.

Fig. 13.19 *Single and double vertical traveltimes in the CFP gather.*

the vertical ray is, by definition, positioned at the correct lateral position.

The focusing operator are defined in single vertical traveltime. The synthesis process converts the two-way time of the data to a mixed version of single and double vertical traveltimes. The single vertical time part of the CFP gather is located at the operator times. The events in the CFP gather above and below the operator times are associated with a double vertical traveltime with respect to the focus point. In figure (13.19) this is explained with a 1 dimensional 3-reflector model. The velocity in the 1 dimensional medium is chosen constant at $c = 2000ms^{-1}$ and at $400, 800$ and $1200m$ (0.4 seconds two-way traveltime) there is a reflector defined by a density contrast. The CFP gather for the first ❶ and third ❸ reflector are shown in figure (13.19) a and b. Looking at the traveltimes for the trace at $x = 0$ it is observed that the time between the layer where the focus point is defined and the other layers is the double vertical traveltime between the layers. This mixture of single and double vertical traveltimes must be used for a proper positioning of the events in-between two focus points defined at the same lateral position but at different depths.

13.2.5 Multi focus CFP-gather

The CFP gather gives the reflection response from one point in the subsurface. The main information in the CFP gather is therefore concentrated around its focus point. It may be useful to search for a gather which contains information about more focus points in one gather. The multi focus CFP-gather (also called X-gather) is constructed by selecting time samples (around the operator times), from different CFP gathers which are constructed with focusing operators defined at the same lateral position but at different depths (or vertical times), and placing these selected time samples in one gather. For example by placing focusing operators, at the same lateral position, at every discrete time position and selecting from the constructed CFP gathers only the time samples at the operator times builds up a multi focus CFP-gather. In the multi focus CFP-gather the samples are renumbered to vertical time with respect to the vertical time of the synthesis operator.

In figure (13.20d) a multi focus CFP-gather at $x = 500$ m is shown for the syncline model. The multi focus CFP-gather is constructed from 4 CFP gathers with their focus points defined at the

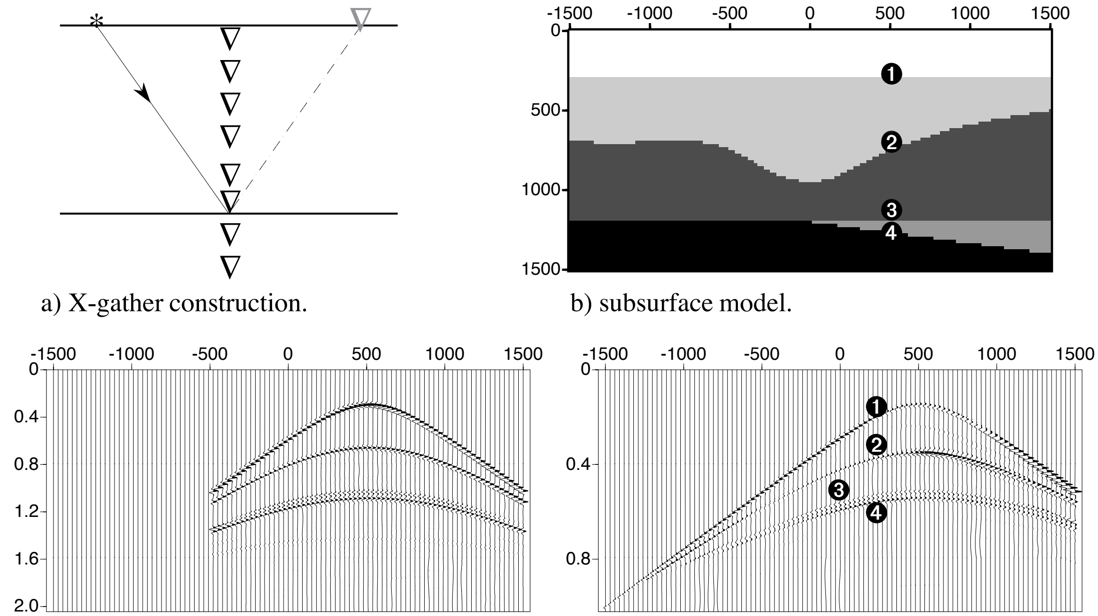

a) X-gather construction.

b) subsurface model.

c) CMP-gather at $x = 500$ m.

d) X-gather at $x = 500$ m.

Fig. 13.20 *For the X-gather at one lateral positions several focus points are defined in depth.*

boundaries of the model. Event ❶ originates from the flat top reflector, ❷ from the right flank of the syncline (note the finite aperture artefact due to the local dip in the layer), ❸ originates from the deep flat reflector (note the negative reflection coefficient) and ❹ from the wedge in the right part of the model. The multi focus CFP-gather can also be used as an alternative for the CMP gather which is shown for comparison in figure (13.20c).

Building the multi focus CFP-gather and using several operators introduces a squeezing of the wavelet at the higher offsets, because at the higher offsets the times of the synthesis operators converge to each other. This squeezed part at the higher offset can be removed from the vertical time image by setting a stretch parameter. In figure (13.20d) the squeezing effect of the wavelet at the higher offsets is clearly visible. In the synthetic example described in section (13.3) more aspects of the multi focus CFP-gather will be explained.

13.2.6 CFP-stack

Correcting a CFP-gather in time with the times defined by the synthesis operator followed by a summation over all traces and placing the result at the vertical operator time (which is the time of the zero-offset trace in the synthesis operator) defines one trace which is called the CFP-stack. The ’stacking’ is done with respect to the times defined by the synthesis operator. The CFP-stack represents the double focusing result at the defined focus point. It is assumed that around the focusing area the obtained image will give a good representation of the area surrounding the focusing point. The area surrounding the focus point is, due to the tube like shape of the focusing beam, good illuminated. This is a very important property from the ef-

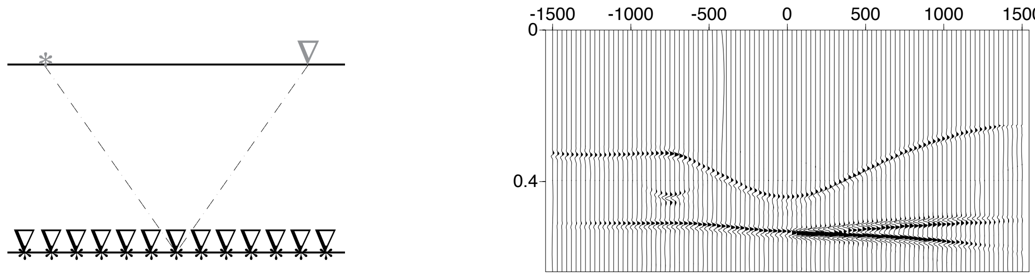

a) CFP-stack construction.

b) CFP-stack at $z = 1200$ m.

Fig. 13.21 *The CFP-stack gives a local image around the defined focus points.*

ficiency point of view. Note that the time samples in the CFP-stack are also renumbered to single vertical time with respect to the vertical time given by the synthesis operator.

Calculating CFP gathers with focus points following, in the lateral direction, a horizon or a reflector followed by the CFP stacking procedure and placing the stacked traces in one file builds up a CFP-stack which 'follows' the boundary. Figure (13.21b) gives a CFP-stack for the focus points positioned at the deep flat reflector in the syncline model. Note that the syncline interface and the wedge are imaged as well. The diffraction point at $x = -750$ is also imaged at the correct lateral position.

13.2.7 Double focusing; imaging in vertical time

The CFP-stack in the previous section represents a local image around the defined focus points. Defining focus points not only at one boundary but in the whole subsurface a complete vertical time image can be build up. As mentioned before it is not necessary to define a focus point at every time position for all lateral positions. Using the information in the focusing beams an optimum focus point distribution can be determined. For the second focusing step at every vertical time sample a synthesis operator is needed. The operators for the second focussing step are obtained by a linear interpolation (in offset or in p) of the operators used in the first focusing step. With these operators the multi focus CFP-gather is move out corrected and stacked. The move out corrected multi focus CFP-gather represents an image gather in vertical time.

The double focusing procedure is explained in figure (13.22) by using the syncline model. For the imaging procedure a focus point is chosen for every lateral position at the three main boundaries in the model. The shot record in figure (13.22a) has a contribution in the CFP gather (constructed with the synthesis operator shown in figure (13.22b)) at its source position $x = -750$, which is indicated by the arrow in (13.22c). The synthesis operator has its focus point defined at $x = 500, z = 1200$. Performing a second focusing step on the CFP gather with the operator of figure (13.22b) and selecting the samples around the operator time gives the contribution indicated by the arrow in figure (13.22d). The lateral position in the image is determined by the lateral position of the synthesis operator. So the information of the event in the shot record indicated by ❹ gives a contribution to the image in figure (13.22d) at $x = 500$ which and is to-

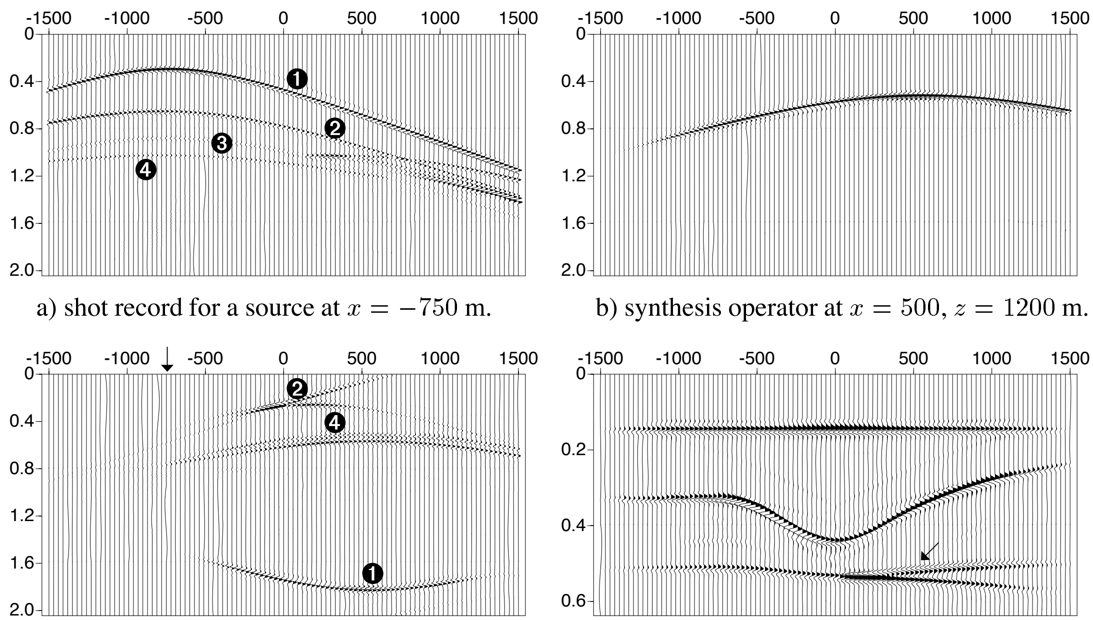

a) shot record for a source at $x = -750$ m.

b) synthesis operator at $x = 500$, $z = 1200$ m.

c) CFP gather.

d) vertical time image.

Fig. 13.22 *The procedure how to obtain from a shot record a double focusing result.*

tally defined by the synthesis operator. The imaging for the samples in between two synthesis operators at the same lateral position is done with interpolated synthesis operator (the second focusing operators). Along the times given by the second focusing operator the samples are stacked and positioned at the correct time position. The time window, which determines which samples are included from the CFP gather in the image, is determined by the time difference between the two operators. Note that due to the fixed spread acquisition geometry the edges of the model are sparsely illuminated.

To show the robustness and sensitivity of the imaging procedure the same imaging procedure is carried out with synthesis operator which are based on a wrong initial macro model. For the erroneous macro model a homogeneous model is chosen with velocity $c = 2200ms^{-1}$ and three depth positions at $z = 400$, $z = 800$ and $z = 1200$ m are chosen for the definition of the synthesis operators. The synthesis operators are generated by using this erroneous macro model and the operators are not updated during in the imaging procedure. Figure (13.23a) shows the CFP-stack for the homogeneous model with only one layer defined at $z = 800$. Figure (13.23b) shows the imaging result with three layers in the homogeneous model. For a good comparison the imaging result using the correct model is shown in figure (13.23c) and the result obtained with conventional prestack depth migration using the correct model is shown in figure (13.23d). Note that the vertical time image obtained with the homogeneous model gives an indication of the reflectors present in the true model. Comparing the depth migration with the vertical time image result shows that if the operators are correct the conversion from the vertical time image to the depth image consists only of stretching the time axis and a lateral shift is not needed.

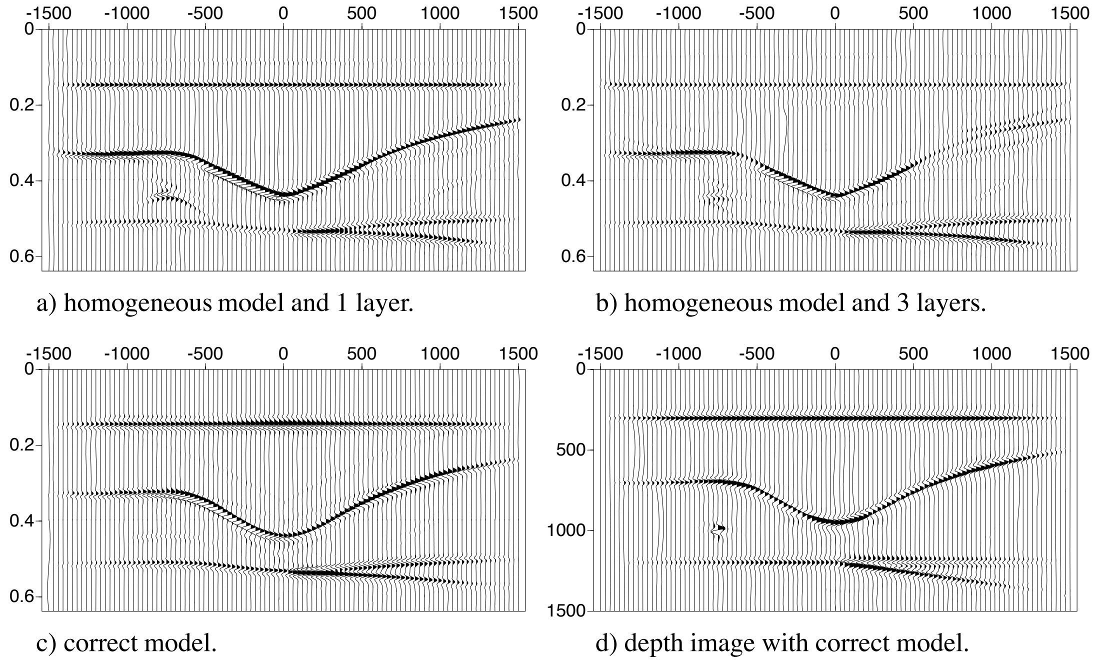

a) homogeneous model and 1 layer.

b) homogeneous model and 3 layers.

c) correct model.

d) depth image with correct model.

Fig. 13.23 *Imaging results for the double focus procedure using synthesis operators based on a homogeneous model; with only one level of focus points (a), with three levels of focus points (b) and the correct model (c). Result (d) shows the pre-stack depth migration result using the correct macro model. Note that result (a) means stacking of CFP gathers.*

Note that the diffraction point is clearly visible in the depth migration and not in the vertical time migration. The vertical time image can be improved by placing an additional focus point at the position of the diffraction point.

The vertical time image can also be build up in another way. After the construction of the CFP-gather, it can be cross-correlated (2-dimensional) with its synthesis operator. This cross-correlation result is placed at the vertical time of the operator and the lateral position of the operator. In the imaging procedure discussed above only the zero-lag trace of the 2D cross-correlation was placed in the imaging result, now every trace is placed in the image. In this way the spatial width of the focus beam can be used in an optimal way and it is not necessary to place at every lateral position a focus point. The result of this imaging procedure is shown in figure (13.24) for different spatial sampling rates for the focusing positions. Note that the vertical time re-sampling is not carried out in the examples shown in figure (13.24). Note also that in figure (13.24) the samples around $t = 0$ represent the correct result which can be used in the vertical time image, the synclinal event at negative times will not be used. For a complete construction of the vertical time image at every boundary focus points must be chosen and combined to construct the image.

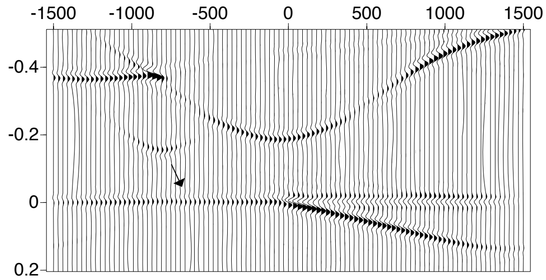

a) Image build with $\Delta x = 15$ m.

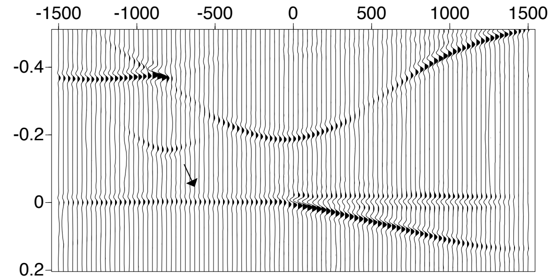

b) Image build with $\Delta x = 45$ m.

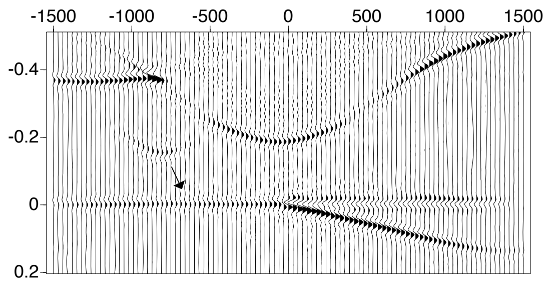

c) Image build with $\Delta x = 75$ m.

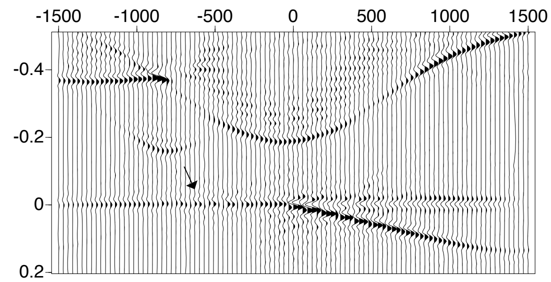

d) Image build with $\Delta x = 105$ m.

Fig. 13.24 *CFP imaging by summing the gridpoint functions for different spacings; the image for the third boundary ($t = 0$) is aimed for only.*

13.2.8 Numerical implementation

The processing based on the CFP technology can be carried out in the traveltime domain, intercept-time domain or frequency domain. The initial synthesis operators used in the examples of this chapter are modeled with a finite difference calculation method based on the software of Vidale (Vidale, 1988). Vidale's method calculates traveltimes through any velocity structure on a two- or three-dimensional numerical grid; amplitudes are not calculated in the program. The traveltime curves of the synthesis operators are stored as single traces in an operator file. In the CFP processing program the synthesis operators are read and stored in an operator table. In the intercept-time algorithm the offset traveltime operators are transformed to rayparameter intercept time operators

For the first focusing step focusing in detection is carried out by default. The focusing in detection for one shot record is carried out for all synthesis operators in the table. For the first synthesis the traces are shifted with the times given by the synthesis operator, followed by weighted addition. The result is positioned at the source location. If the time given by the synthesis operator does not fit on the discrete time-grid of the shot record a linear interpolation to the operator time is carried out. An option for the first focusing step is a double vertical time display, meaning that the CFP gather is delayed with the single vertical time at the focus point position. Another option performs an move out correction on the CFP gather based on the synthesis operator. If the synthesis operator fits the data then a flat event is produced and it is positioned at the (single or double) vertical time of the focus point position.

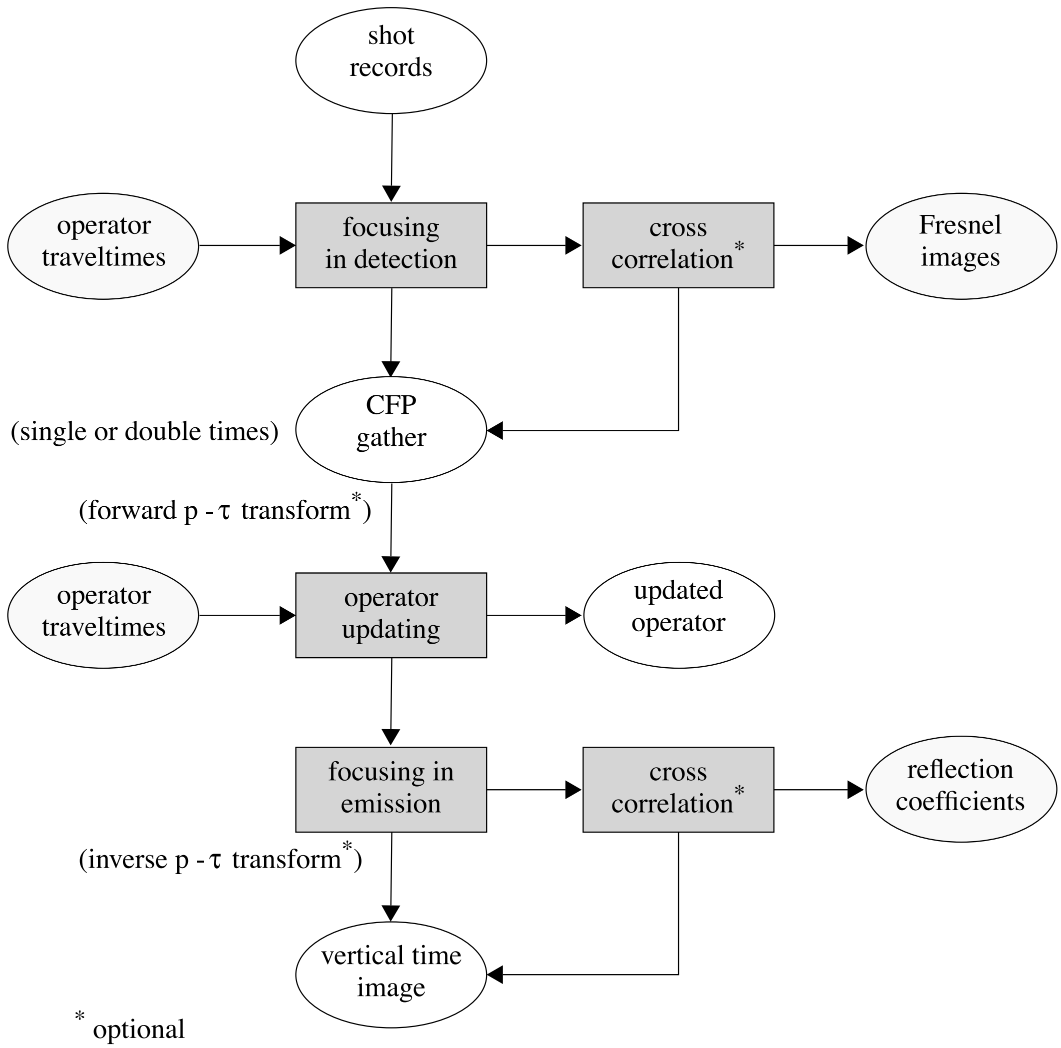

Fig. 13.25 *Schematic representation of the CFP algorithm in the time domain. Note that the processing is done in a shot gather stream, which makes the data in and output straightforward.*

In the second focusing step a synthesis operator is needed for every vertical time sample. The synthesis operators in between two focus points are obtained by linear interpolation of the operator times. With these operators the second focusing step is carried out by a summation along the (interpolated) operator times. The result is positioned at the lateral position of the focus point and at the vertical time of the synthesis operator.

The flow scheme of the synthesis algorithm is shown in figure (13.25). In this scheme it is possible to include all kinds of data-control during the processing. In the first focusing step a window around the operator times can be selected, to allow operators errors to be evaluated. Every CFP gather can be build up from all shot records around the focus point as determined by the source aperture. The result of the focusing in detection can be compared with the traveltime operator and CFP gather can be updated. The cross-correlation of the operator and the data makes it possible to interpolate for irregular and/or large source spacing (this is investigated in the acquisition consortium). The CFP-stack and multi focus CFP-gather are special selections of the different options shown in the scheme.

In the list below the most important parameters used in the CFP software are explained:

① **focus point sampling in vertical time ΔT .**
In the synthesis operator generation for the first focusing step the vertical time distance between two synthesis operators has to be defined. The value of ΔT determines the sampling of the focus points in vertical time. It is not necessary to place at every sample position a focus point; typically ΔT ranges from 40 to 100 ms!.

② **stretch factor**
The move out corrected multi focus CFP-gather (which is the CFP image gather) introduces a stretching of the wavelet at the higher offsets (typical for move out corrections). This part at the higher offsets can be removed prior to stacking by setting the stretch parameter (similar to NMO correction).

③ **source aperture**
The source aperture is given in angles (typical is 60^o); it determines the number of shots to be included for a certain focus point.

13.3 Synthetic example

The 1-dimensional shot record shown in figure (13.26a) is based on a well log shown in figure (13.26b) and is used as input data for the CFP processing scheme. Due to the presence of the many layers in the model this synthetic data set can be used to clarify the concept of multi focus CFP-gathers (X-gathers). Choosing a synthesis operator at the top (❶), middle (❷) and bottom (❸) of the model and re-numbering the constructed CFP gather to single vertical times gives the results shown in figure (13.26)d, e and f. The re-numbering is carried out with respect to the traveltime between the focus point and the source position at the surface (this time is given by the synthesis operator).

In figure(13.26) d, e and f it is observed that in the focusing area of the synthesis operator the renumbered CFP-gather gives a good representation of the subsurface. Further away from the focusing area the construction is less accurate and finite aperture artefacts distort the data. Constructing a move out corrected multi focus CFP-gather from these gathers is carried out by a time correction given by the interpolated synthesis operator followed by a summation over all traces. This construction is shown in steps in figure(13.26) g, h and i. In figure(13.26) g the three single focus gathers d, e and f are combined to one multi focus CFP-gather. This is done by combining the samples around a window of the synthesis operator times and placing these selections into one file. The CFP-stack is constructed from figure(13.26) g by an move out correction given by the synthesis operator and a summation over all traces. The result before

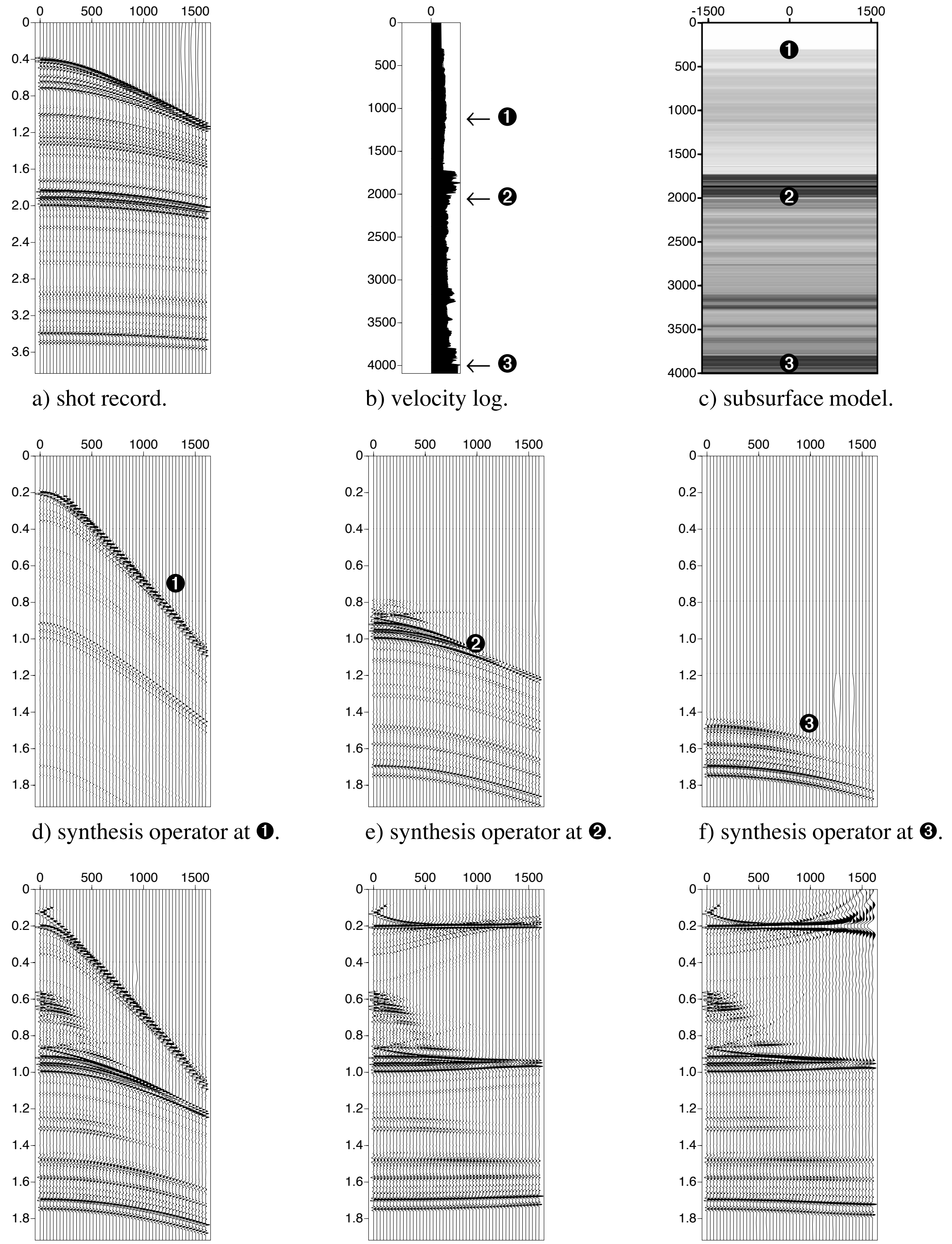

a) shot record.
b) velocity log.
c) subsurface model.
d) synthesis operator at ❶.
e) synthesis operator at ❷.
f) synthesis operator at ❸.
g) combination of ❶+❷+❸.
h) move out correction of g.
i) CFP image gather.

Fig. 13.26 *X-gathers in a 1-dimensional medium. The arrow indicates where the focus points are chosen. Note the construction of the move out corrected X-gather from figure g to i. It is interesting to see that only 3 focus points yield already reasonable results.*

summation is shown in figure(13.26) h. In this figure the events at the operator times are perfectly flat and will give a good representation of the reflector present at the focus point. In the second focusing step a synthesis operator is needed at every time sample. These synthesis operators are obtained by interpolating the operators from the first focusing step.

The result of the second focusing step is shown in figure(13.26) i. In this gather the events around the focusing point are aligned, the events in between focus points are only for the deeper events good aligned. The operators which have focus points at deeper structures give a better alignment due to the smaller move out correction for the higher offsets. The shallow part shows a significant stretching for the higher offsets occurs due to the convergence of the time curves of the synthesis operators at higher offsets. The stretched events are normally not included in the construction of the image and are muted out for stretch vales greater than a certain threshold.

In figure (13.27)a the perfect move out corrected X-gather is shown (which is for the one dimensional medium equal to the zero offset trace displayed in single vertical time). By constructing X-gathers with different sampling rates in vertical time of the synthesis operators in the first focusing step and comparing these results with the perfect double focus gather gives an indication of the focusing area of the synthesis operators. Comparing the results of figure(13.27) g, h and i with the double focus gather in figure(13.27a) shows already that three synthesis operators are not sufficient to illuminate the whole depth range. However, for the focusing operators in the deeper parts of the model the focusing area is bigger than for a focusing operator close to the surface. Note that the CFP image gathers clearly identify that the focusing operators around 1 second are not correct.

By selecting a focusing operator at every 32 ms (single vertical time) in the subsurface a better double focus gather is build up which is shown in figure(13.27b). Note that in this gather the stretched events, which are normally not included, are shown here for a better comparison. To connect the contributions from the different CFP gathers an overlapping window with a cosine taper is used. By placing the synthesis operators at different vertical time distances different double focus gathers can be build and compared with each other to determine a sampling density for the synthesis operators which is sufficient to image all events present in the data. In figure (13.27) several double focus gathers are shown for different sampling rates of the synthesis operators in the first focusing step. Comparing the results indicates that a sampling of 64 or 128 ms is sufficient to illuminate all events in between the defined operators.

13.4 Field data example; Mobil data set

The Mobil data-set is often used in the DELPHI program. The initial macro model was estimated with the areal shot record technology as proposed in DELPHI volume V, Chapter 10. Now we are using our CFP move out analysis based on the theory in Chapter 9. The estimated macro model consists of seven macro layers. For a detailed description of the velocity analysis on the Mobil data set the reader is referred to Chapter 7. Note that the macro model is estimated by using the same CFP technology, this makes the macro model estimation and the imaging closely connected to each other. For example model errors observed in the construc-

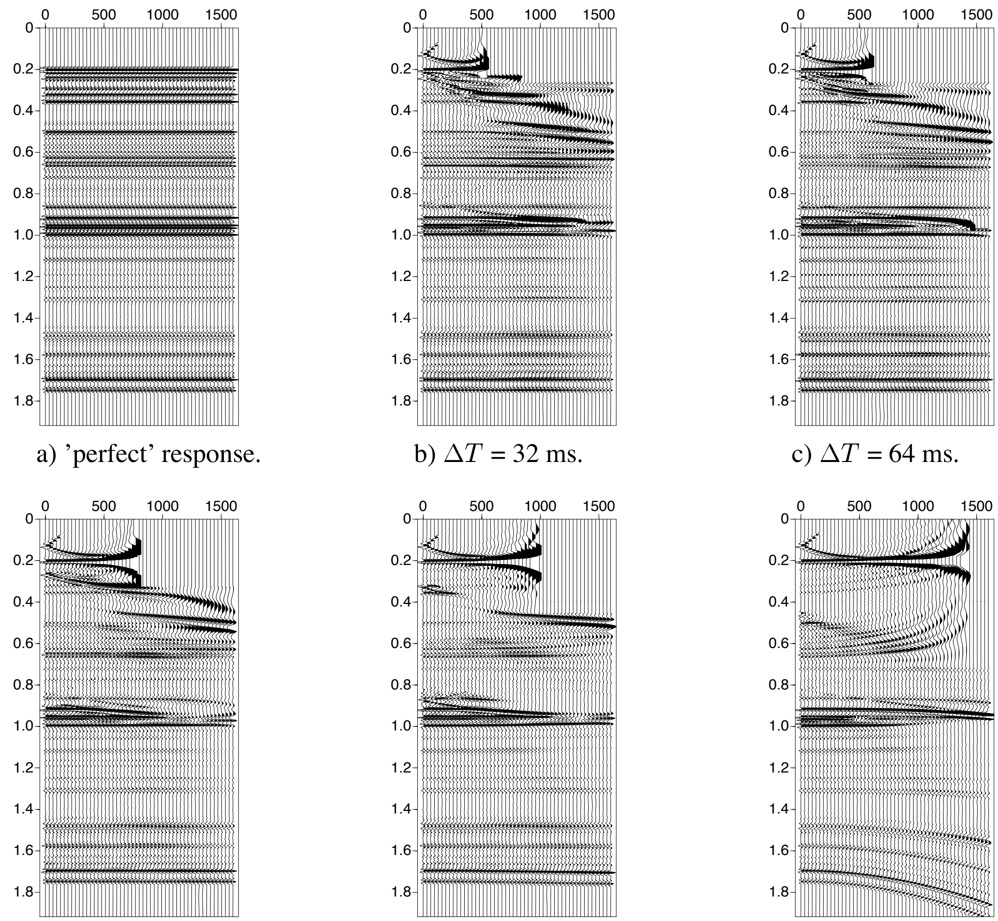

a) 'perfect' response. b) ΔT = 32 ms. c) ΔT = 64 ms.

d) ΔT = 128 ms. e) ΔT = 256 ms. f) ΔT = 512 ms.

Fig. 13.27 *CFP image gathers in a 1-dimensional medium for different sampling rates, in single vertical time, of the synthesis operators. Note that the CFP image gathers clearly indentify that the focusing operators around 1 second are not correct.*

tion of the image can be directly used to update the macro model.

The data set contains two well positions within the seismic line. The CFP analysis presented in this chapter is concentrated on these two well positions. For a first analysis focusing beams are calculated for focus points at every macro boundary below the two well positions A and B (for a detailed description of the positions of the wells the reader is referred to Chapter 7). In figure (13.28) the beams and the synthesis operators are shown. The beams show the focusing of energy, for the different synthesis operators, at the defined macro boundaries. Note that in between the boundaries the illumination energy is not sufficient to image the events in between the boundaries. So for a good first focusing step more operators are needed as used in figure (13.28).

For a better analysis of the illumination energy different beams are calculated where the dis-

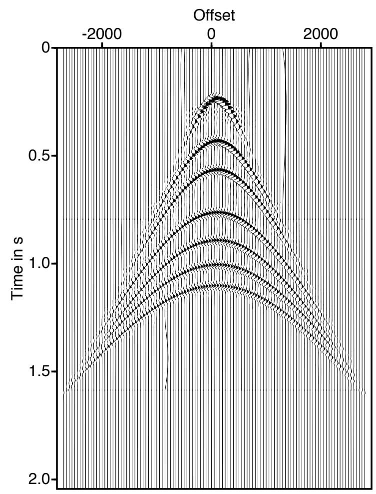

a) X-operator at well A.

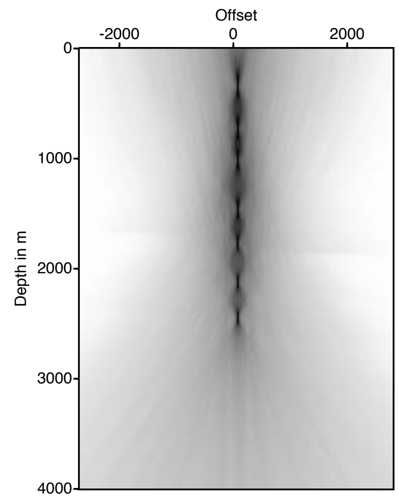

b) X-beam at well A.

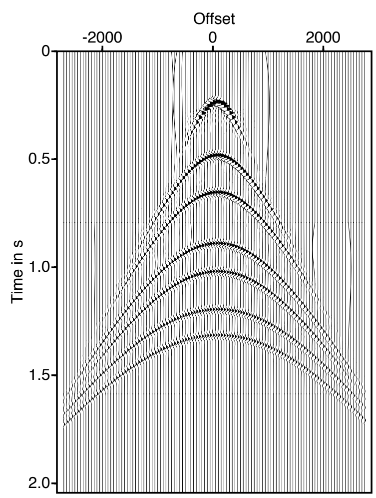

c) X-operator at well B.

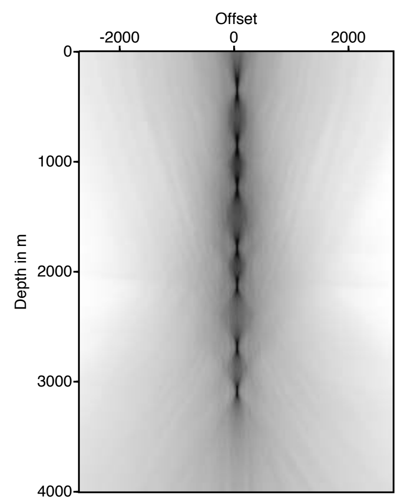

d) X-beam at well B.

Fig. 13.28 *Focussing operators and beams for focus points at every macro boundary at the positions of the wells.*

tance between the focus points in depth is changed. The results of these experiments are shown in figure (13.29). In figure (13.29) the contribution of the different beams is limited to its focusing area, in figure (13.28) the beams of the individual focus points are just added together. The different beams show that close to the surface energy is reduced due to the limited aperture range and the energy for the deeper part of the model is reduced due to the spherical difference of the wavefront. It is also observed that a sampling rate of $\Delta z = 100$ m show a beam which is continuous in depth. From these experiments it is concluded that for $\Delta z = 200$ m a sufficient illumination is obtained.

An X-gather is defined at the position of well A and well B and is constructed with synthesis

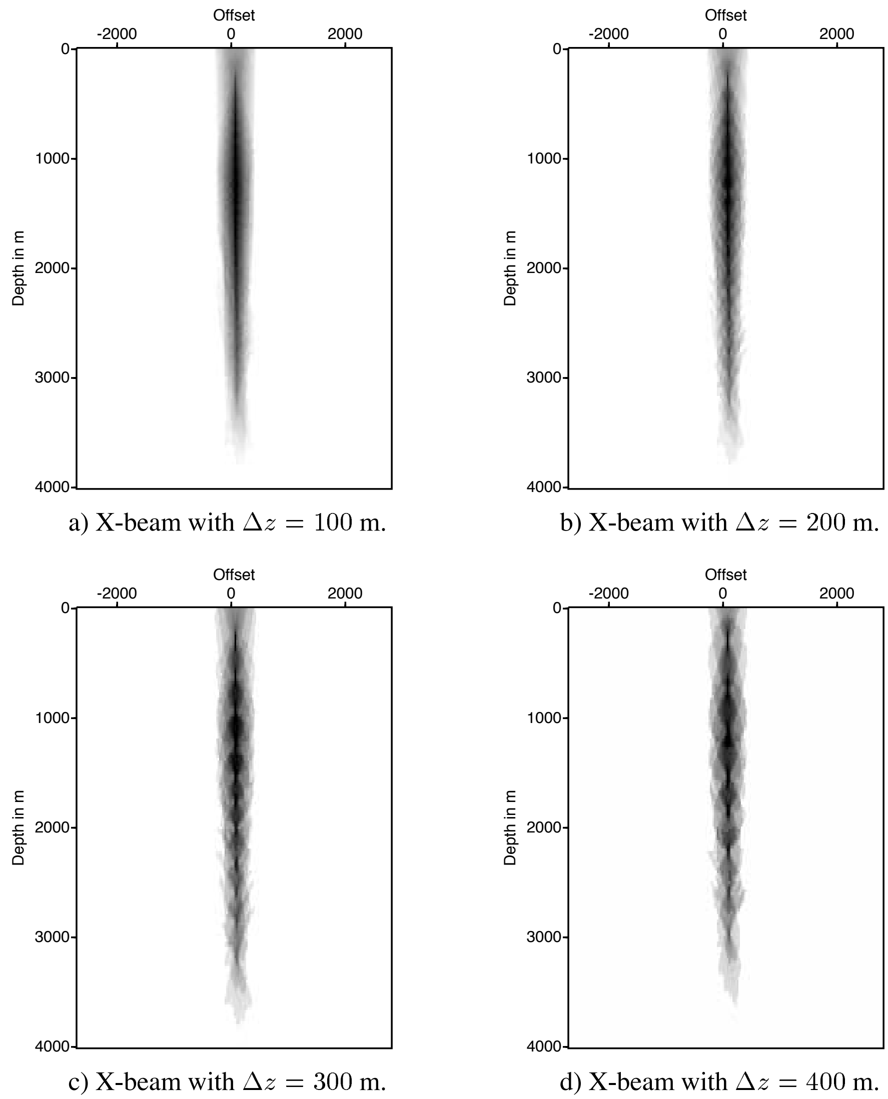

a) X-beam with $\Delta z = 100$ m.
b) X-beam with $\Delta z = 200$ m.
c) X-beam with $\Delta z = 300$ m.
d) X-beam with $\Delta z = 400$ m.

Fig. 13.29 *X-beams for a set of focus points at the same lateral positions (well B) but with a different sampling rate in depth.*

operators defined for focus points with a sampling rate of $\Delta z = 200$. Figure (13.30) shows the X-gathers and the CMP gathers for the same position. The CMP gather is displayed with same time sampling and offset range as the X-gather. Note that the first 10 traces (until offset 250 m) in the CMP gather are interpolated traces, the X-gathers are constructed without the interpolated traces. Note that for the higher offsets the X-gather shows more continued events than the CMP gather.

The X-gathers are the input for the second focusing step. In figure (13.31) for both well positions the move out corrected X-gathers (CFP image gathers) are shown; one with synthesis operators defined at every 200 ms and one with operators defined at every 80 ms. With these

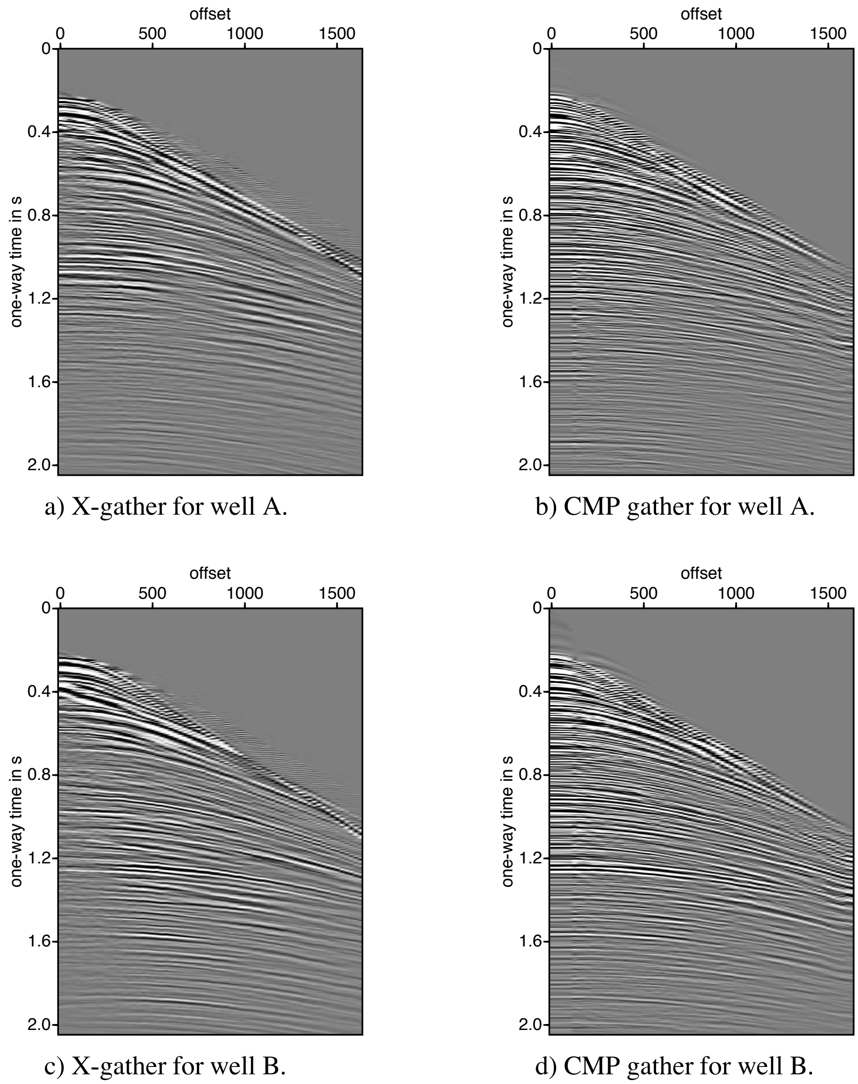

Fig. 13.30 *X-gathers and CMP gathers at the positions of well A and well B. Note that the first 10 traces in the CMP gather are interpolated traces.*

operators CFP's are calculated. The interpolated traces are not used in the calculation and an overlapping area of 10 sample points is used between two adjoined CFP gathers. In the CFP image gathers the good alignment of the events is observed. Note that for the shallow part more operators are needed than for the deeper part. It is therefore more efficient to use operators which are differently sampled in vertical time. However if one is only interested in the lower part the operators at the surface need not to be calculated.

The CFP migration result is shown is figure (13.32). The migration result is obtained with synthesis operator sampled with 80 ms in single vertical time, which is equivalent with a depth step of $\Delta z = 200$ m. Due to the tube like shape of the focusing beams this is sufficient to obtain a good image of the subsurface. The CFP migration is therefore more efficient than conventional prestack depth migration.

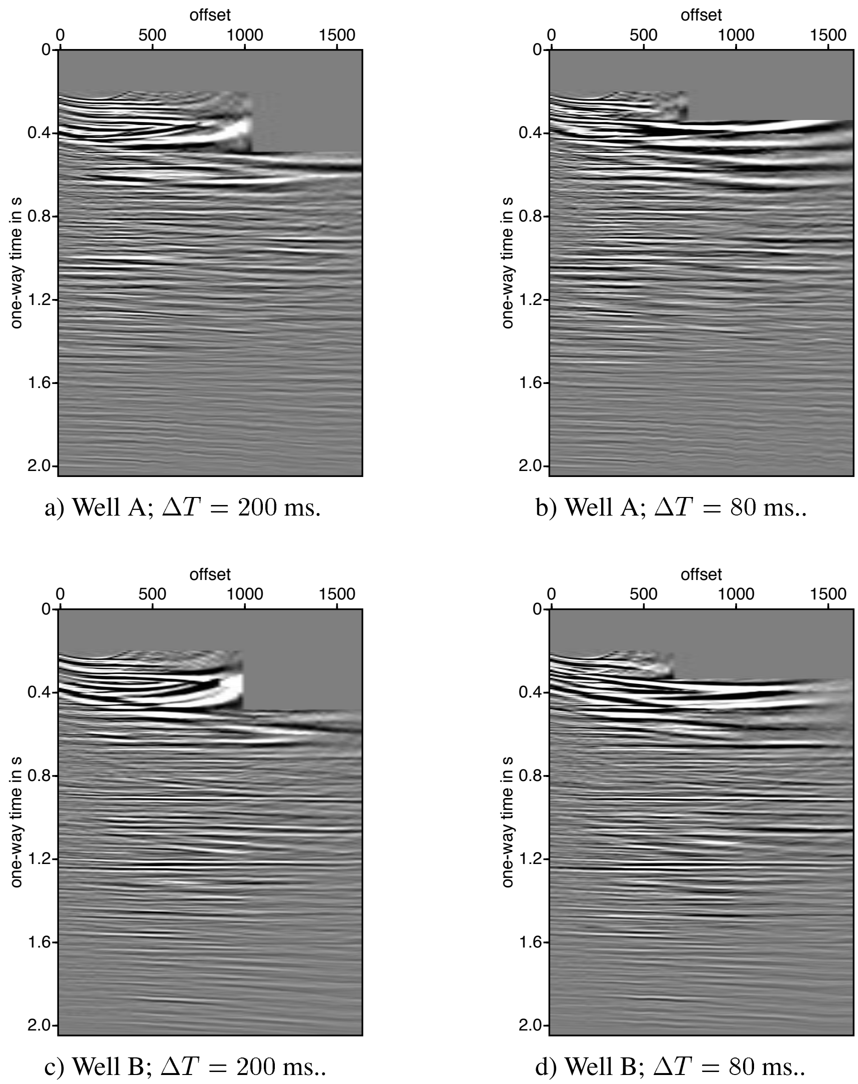

Fig. 13.31 *CFP image gather at the positions of well A and well B for different sampling rates of the defined focus points.*

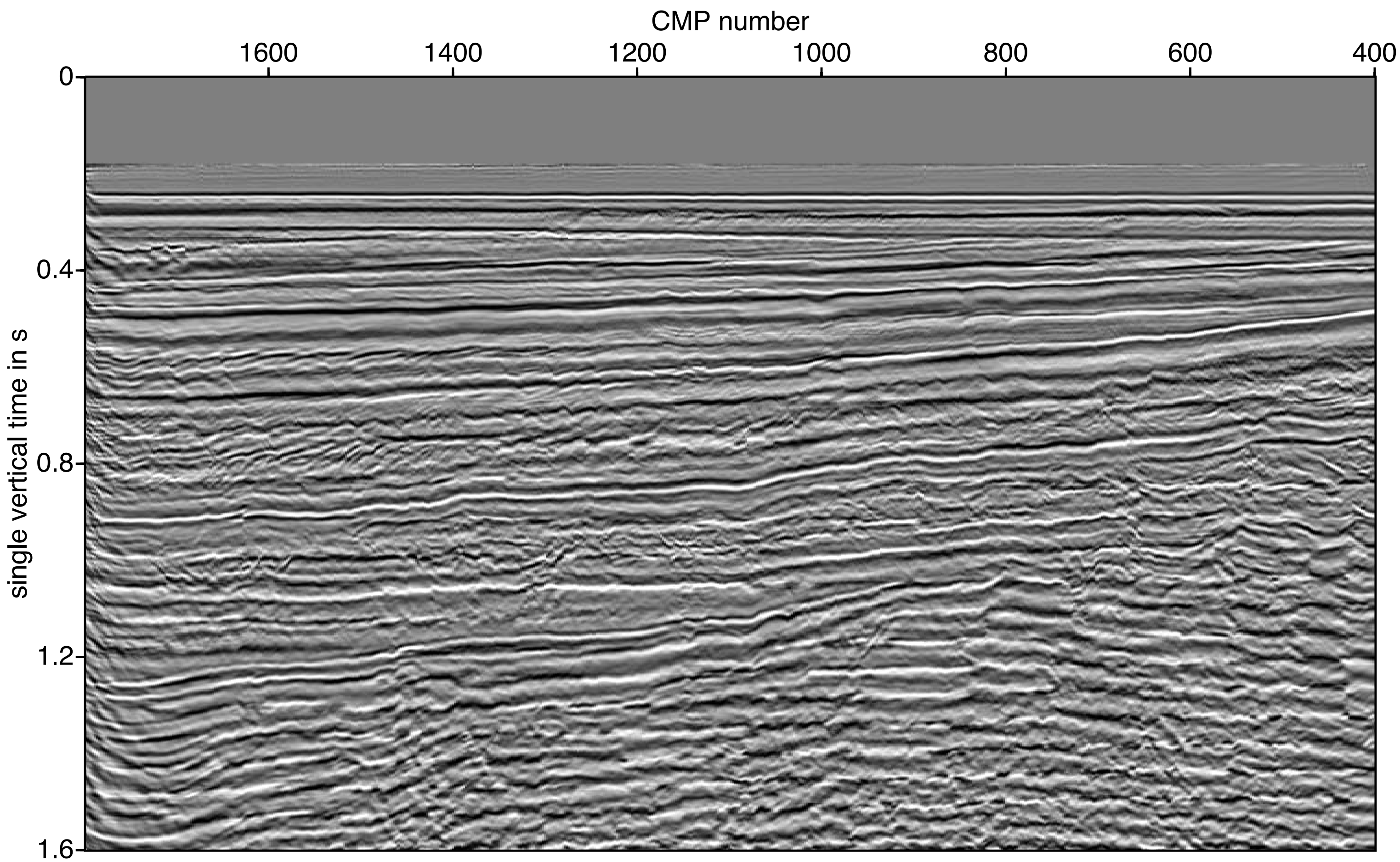

Fig. 13.32 *Prestack migration result obtained with the CFP velocity analysis and migration method. Note that only a limited number of operators is used to construct the complete image:* $\Delta T = 80$ *ms.*

13.5 Future developments

In the coming year the following subjects will be investigated:

① Refinements in the choice of ΔT (first focusing step) and the stretching factor (second focusing step).

② Automatic updating of CFP gather (by convolution) and CFP operator (by correlation)

③ CFP gathers in 3D acquisition geometry, including multi-spread/ multi-streamer.

13.6 Discussion and conclusions

The examples in this chapter have demonstrated that the double focusing concept is a very effective and efficient way of applying prestack migration. The vertical area surrounding the focus point in the first focusing step is, due to the tube-like shape of the focusing beam, well illuminated. Therefore only a limited number of synthesis operators is needed in the first focusing step to illuminate the complete subsurface. This is a very important property of the CFP method from an efficiency point of view.

13.7 References

Berkhout, A. J., 1992, Areal shot record technology: Journal of Seismic Exploration, **1**, no. 2, 251–264.

Parkes, G., and Hatton, L., 1987, Towards a systematic understanding of the effects of velocity model errors on depth and time migration of seismic data: First Break, **5**, no. 4, 121–133.

Rietveld, W. E. A., 1995, Controlled illumination in prestack seismic migration: Ph.D. thesis, Delft University of Technology.

Vidale, J., 1988, Finite-difference calculation of travel times: Bulletin of the Seismological Society of America, **78**, no. 6, 2062–2076.

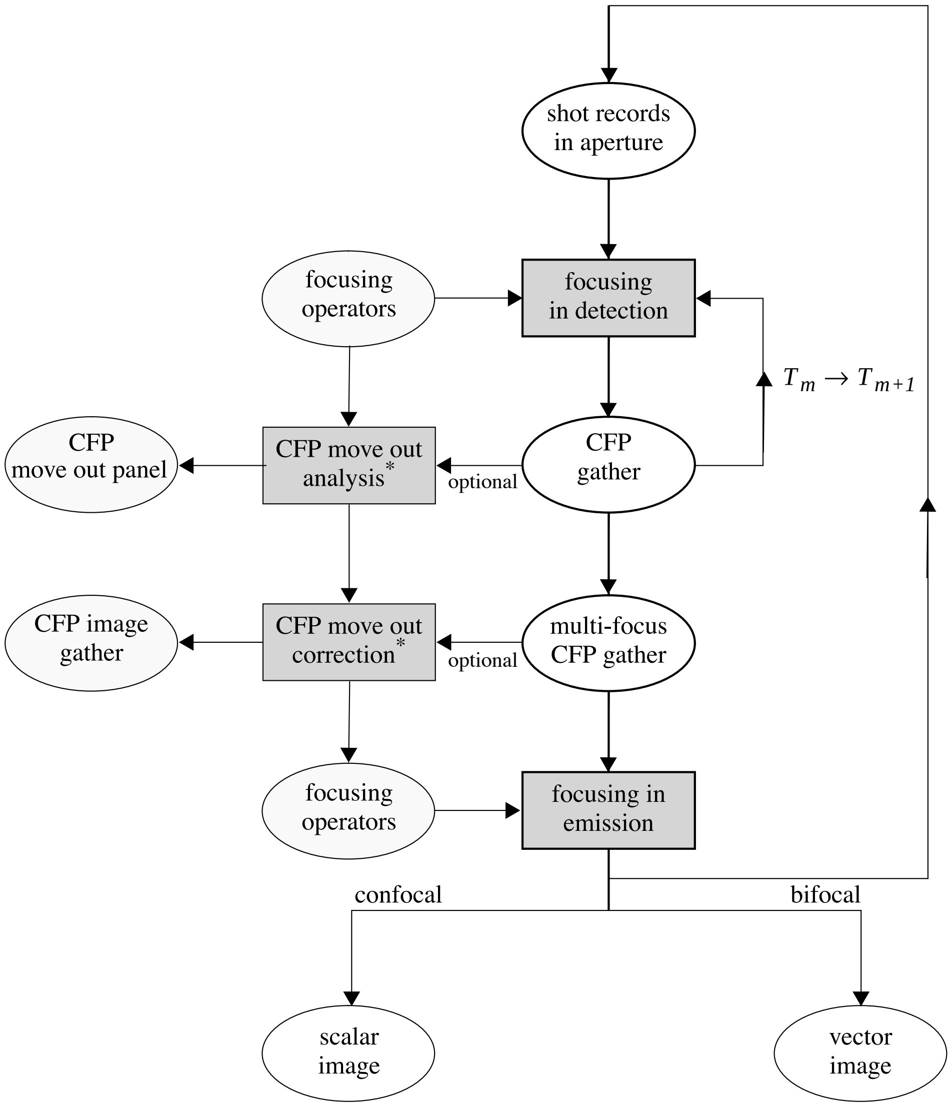

* optionally in p - τ

Fig. 13.33 *CFP processing scheme.*

Contents